Human brown adipose tissue is phenocopied by classical brown adipose tissue in physiologically humanized mice

Jasper M. A. de Jong[1,12], Wenfei Sun[2], Nuno D. Pires[2], Andrea Frontini[3], Miroslav Balaz[2], Naja Z. Jespersen[4,5], Amir Feizi[6], Katarina Petrovic[7], Alexander W. Fischer[1,8,13,14], Muhammad Hamza Bokhari[1], Tarja Niemi[9], Pirjo Nuutila[10], Saverio Cinti[11], Søren Nielsen[4], Camilla Scheele[4,5], Kirsi Virtanen[10], Barbara Cannon[1], Jan Nedergaard[1], Christian Wolfrum[2] and Natasa Petrovic[1]*

Human and rodent brown adipose tissues (BAT) appear morphologically and molecularly different. Here we compare human BAT with both classical brown and brite/beige adipose tissues of 'physiologically humanized' mice: middle-aged mice living under conditions approaching human thermal and nutritional conditions, that is, prolonged exposure to thermoneutral temperature (approximately 30 °C) and to an energy-rich (high-fat, high-sugar) diet. We find that the morphological, cellular and molecular characteristics (both marker and adipose-selective gene expression) of classical brown fat, but not of brite/beige fat, of these physiologically humanized mice are notably similar to human BAT. We also demonstrate, both in silico and experimentally, that in physiologically humanized mice only classical BAT possesses a high thermogenic potential. These observations suggest that classical rodent BAT is the tissue of choice for translational studies aimed at recruiting human BAT to counteract the development of obesity and its comorbidities.

Within the last decade, the presence and metabolic activity of BAT has been unequivocally demonstrated in adult humans[1–6]. This has created appealing perspectives to recruit and activate brown and browning-competent adipose tissues to counteract the development of obesity and its comorbidities in adult humans (for example, see refs. [7–11]).

It is of the utmost importance for translationally focused research that it should be performed under conditions that, as far as possible, are relevant to humans. In particular, it is debatable whether routinely used, young, chow-fed mice living under conditions of constant cold stress (as in 'standard' housing conditions) are physiologically relevant metabolic models for middle-aged humans chronically fed tempting diets and living predominantly under thermoneutral conditions. Indeed, a series of studies indicate the substantial effects of the cold-induced metabolic stress experienced by mice at room temperature on areas as different as cancer, cardiovascular function and response to infectious agents[12–14]. Particularly in studies regarding heat-producing brown and brite/beige adipose tissues, it may be anticipated that not only food and age, but particularly thermal conditions may substantially affect the state of tissues.

A key question in the field of brown and brite/beige adipose tissues concerns the 'identity' of human BAT in relation to murine classical brown and brite/beige adipose tissues. An influential paper, based on elegant molecular studies of cloned immortalized cells originating from mouse brite/beige and classical BAT, concluded that brite/beige rather than classical BAT was the preferred model for human BAT[15] (see also Sharp et al.[16]). Subsequent studies have suggested the presence of molecular signatures in human BAT indicative of both murine classical brown and brite/beige fat[17–19]. Given the developmental and potential functional differences between murine classical brown and brite/beige adipose tissues, it is highly important to reveal the true nature of human BAT, in order to conduct translational studies in mice. In the present study, in direct comparison with verified human BAT, we examined whether the use of 'physiologically humanized' mice— that is, mice living under conditions approaching human thermal and nutritional conditions—may influence the conclusions about the nature of human BAT. We found this to be the case.

Results

Interscapular BAT (iBAT) in thermoneutral mice morphologically phenocopies human BAT. An example of the appearance of

[1]Department of Molecular Biosciences, The Wenner-Gren Institute, Stockholm University, Stockholm, Sweden. [2]Institute of Food, Nutrition and Health, Eidgenössische Technische Hochschule Zürich, Schwerzenbach, Switzerland. [3]Department of Public Health, Experimental and Forensic Medicine, University of Pavia, Pavia, Italy. [4]The Centre of Inflammation and Metabolism and Centre for Physical Activity Research Rigshospitalet, University Hospital of Copenhagen, Copenhagen, Denmark. [5]Novo Nordisk Foundation Center for Basic Metabolic Research, Faculty of Health and Medical Sciences, University of Copenhagen, Copenhagen, Denmark. [6]Novo Nordisk Research Centre Oxford, Oxford, UK. [7]Department of Chemistry, School of Engineering Sciences in Chemistry, Biotechnology and Health, KTH Royal Institute of Technology, Stockholm, Sweden. [8]Department of Biochemistry and Molecular Cell Biology, University Medical Center Hamburg-Eppendorf, Hamburg, Germany. [9]Department of Surgery, Turku University Hospital, Turku, Finland. [10]Turku PET Centre, University of Turku, Turku, Finland. [11]Department of Experimental and Clinical Medicine, University of Ancona, Ancona, Italy. [12]Present address: Department of Comparative Medicine, Yale School of Medicine, New Haven, CT, USA. [13]Present address: Department of Genetics and Complex Diseases, Harvard T. H. Chan School of Public Health, Boston, MA, USA. [14]Present address: Department of Cell Biology, Harvard Medical School, Boston, MA, USA. *e-mail: natasa.petrovic@su.se
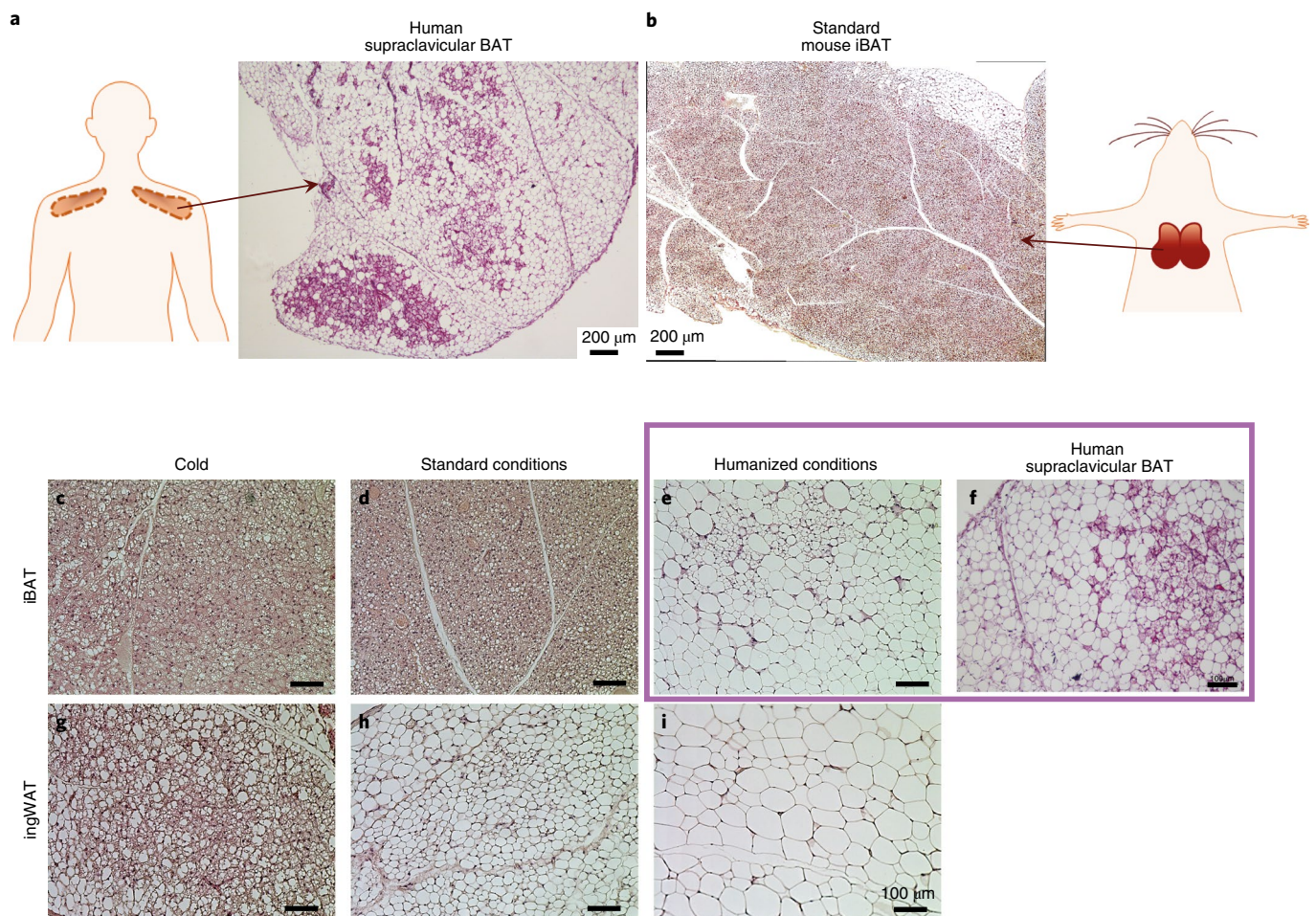
Fig. 1 | iBAT in physiologically humanized mice morphologically phenocopies human supraclavicular BAT. a, Histological appearance of human supraclavicular BAT. Scale bar, 200 μm. **b**, Histological appearance of iBAT of 8-week-old C57BL/6 mice on a chow diet at a temperature of 21 °C. Scale bar, 200 μm. **c,g**, Histological appearance of iBAT (**c**) and ingWAT (**g**) of 14-week-old C57BL/6 mice on a chow diet and acclimated to a temperature of 4 °C for 4 weeks. **d,h**, Histological appearance of iBAT (**d**) and ingWAT (**h**) of 8-week-old C57BL/6 mice on a chow diet at a temperature of 21 °C. **e,i**, Histological appearance of iBAT (**e**) and ingWAT (**i**) of 45-week-old C57BL/6 mice on a high-fat diet at thermoneutrality for 33 weeks. Scale bar, 100 μm. **f**, Histological appearance of human supraclavicular BAT, the same as in **a**, but the image was captured at a higher magnification. Scale bar, 100 μm. **b–d,g,h**, Images are representative of at least two independent biological samples. **e,i**, Pictures are representative of at least five independent biological samples. **a,f**, A single human supraclavicular BAT was analysed, but see earlier similar images[6].

human BAT from the supraclavicular region is presented in Fig. 1a. Histological examination by haematoxylin and eosin staining revealed lobular subdivisions containing distinct islands of densely stained adipocytes surrounded by lipid-filled unilocular adipocytes, as has been reported elsewhere[2–6,17–19]. The morphological appearance of mouse iBAT—as studied routinely–is entirely different (Fig. 1b). Mouse BAT essentially comprises only small multilocular brown adipocytes that are distributed uniformly throughout the tissue (Fig. 1b,d). This BAT morphology is considered 'typical' (Fig. 1b,d) given that the majority of current mouse studies are performed under such standard conditions. Thus, in mice living under mild cold conditions (21 °C) (Fig. 1b,d) (or under more extreme cold conditions (4 °C) (Fig. 1c)), the tissue appears morphologically very different from human BAT (Fig. 1a).

Since this standard housing temperature for mice (approximately 20 °C) is about 10 °C below their thermoneutral temperature (approximately 30 °C), it imposes significant thermal stress and leads to constantly activated thermoregulatory thermogenesis[20]. Therefore, we performed histological examination of BAT from mice that had been living under conditions approaching human thermal (thermoneutrality) and nutritional (exposure to an

energy-rich diet) conditions for a prolonged period of time (6–8 months). When the experiments started, mice were 12 weeks old, that is, fully developed; when examined, they were about 9–11 months old, that is, middle-aged. Even though these conditions do not mimic the subtle variations in temperature and food composition that humans are usually exposed to, they still represent the best controllable and experimentally achievable approximation of human conditions—both mice at thermoneutrality and humans given the possibility to be at any temperature have 'physical activity levels' of approximately 1.7[21]. Therefore, we refer to these thermoneutral, 'Western diet'-fed middle-aged mice as physiologically humanized, in contrast to standard mice that are young, chow-fed and constantly cold-exposed.

In these physiologically humanized mice, histological analysis revealed features of BAT morphology that would be considered atypical for classical BAT. In most areas, tissue appearance was much more similar to the standard appearance of mouse white adipose tissue (WAT) than to the appearance of BAT from mice living at standard temperatures (20–22 °C) (Fig. 1e). Such altered morphology was noted in certain earlier studies[22–26]. Adipocytes were large and unilocular and thus had the appearance of white adipocytes;

however, they were noticeably smaller (average diameter approximately 25 μm) than classical white adipocytes in the same animals (average diameter approximately 70 μm (ref. [27])). In some regions of the tissue, occasional multilocular adipocytes, usually organized in islands surrounded by unilocular adipocytes, were observed (Fig. 1e). Thus, the classical BAT of the physiologically humanized mice was composed of both unilocular adipocytes and islands of multilocular adipocytes, demonstrating remarkable morphological similarity to human supraclavicular BAT (compare with Fig. 1e,f).

Based on the molecular evidence that brite/beige adipose tissue may be the mouse equivalent of human BAT[15,16], we examined inguinal WAT (ingWAT), the largest browning-competent mouse adipose depot and the one that shows the strongest browning potential[28,29]. The ingWAT of mice exposed to standard conditions was essentially composed of only unilocular adipocytes; only few multilocular adipocytes were observed (Fig. 1h). However, in mice acclimated to cold (4 °C), multilocular adipocytes were much more frequent (Fig. 1g) and were found in islands surrounded by unilocular adipocytes. This particular type of adipocytes—occurring in white adipose depots upon chronic sympathetic stimulation but possessing characteristics of brown adipocytes–have been named brite[30] or beige[31]. Under these conditions, the ingWAT (Fig. 1g) was thus morphologically similar to human BAT (Fig. 1f). However, in physiologically humanized mice, all adipocytes within the browning-competent ingWAT were unilocular (Fig. 1i) and were larger than in mice living under standard conditions (Fig. 1i compared to 1h).

Thus, the classical BAT of physiologically humanized mice (Fig. 1e) and human supraclavicular BAT (Fig. 1f) were morphologically similar and composed of both unilocular and multilocular adipocytes. The diameters of the unilocular and multilocular adipocytes in human BAT were similar to the diameters of the unilocular and multilocular adipocytes in humanized mouse BAT. The brite/beige adipose tissue of mice acclimated to cold (Fig. 1g) displayed similar morphology, but achieving this morphology required intense cold stimulation.

Humanized mouse iBAT retains a distinct 'thermogenic' molecular signature. Since the brown fat of physiologically humanized mice (Fig. 1e) morphologically resembled WAT, the question may be asked whether it retained the molecular properties defining brown fat. Therefore, we examined brown fat-specific characteristics at the molecular and cellular levels.

The expression of functional brown fat-specific/enriched genes was readily detected in the iBAT of mice living under humanized conditions (Fig. 2a, brown squares). However, as expected, and in agreement with earlier studies (for example, see refs. [25,28,32,33]), expression levels in these mice were significantly lower than in the thermogenically recruited brown fat of mice living under standard conditions (Fig. 2a, brown circles; note the logarithmic scale on the y axes). Also as expected, the expression of these thermogenesis-related genes was generally two orders of magnitude lower in standard ingWAT than in standard iBAT (Fig. 2a, orange circles), and the expression levels were further decreased upon 'humanization' (Fig. 2a, orange squares).

The data presented in Fig. 2a were analysed using hierarchical cluster analysis (Fig. 2b). The resulting heatmap demonstrates that all ingWAT samples were grouped in the same cluster. In contrast, humanized and standard iBAT samples formed two separate clusters (the humanized iBAT samples were hierarchically closer to ingWAT than standard iBAT). Thus, humanization led to more pronounced changes in iBAT than in ingWAT.

Humanized mouse iBAT is as heterogeneous as human BAT. Immunohistochemical analysis of human supraclavicular BAT revealed that uncoupling protein 1 (UCP1) is not homogeneously distributed; only certain multilocular adipocytes expressed UCP1 (Fig. 2f and[2–6,17–19]). To examine the effect of physiological humanization on mouse brown adipocyte-specific characteristics at a cellular level, particularly the distribution of thermogenesis-competent adipocytes, mouse depots were studied with immunohistochemistry for UCP1; counterstaining for perilipin enabled visualization of each adipocyte within the tissues. Notable similarity between human BAT and the BAT of physiologically humanized mice was observed (Fig. 2f versus 2e). Thus, also in the BAT of physiologically humanized mice, UCP1 was not homogeneously distributed; only multilocular adipocytes were evidently UCP1^{+} (Fig. 2e). This was very distinct from the appearance of the cells in mice living under standard conditions (Fig. 2d) or in chronic cold (Fig. 2c) where UCP1^{+} adipocytes were distributed uniformly throughout the BAT.

In ingWAT, UCP1^{+} adipocytes were found only in cold-acclimated mice; only certain multilocular adipocytes were UCP1^{+} (Fig. 2g). UCP1^{+} cells were not present at all in ingWAT in mice living under standard or humanized conditions (Fig. 2h,i).

Thus, brown fat in humans displays remarkable cellular similarity to the brown fat of thermally and nutritionally humanized mice. Under these humanized conditions, no cellular similarity of human brown fat to the browning-competent ingWAT adipose depot was observed.

Brown versus brite/beige marker genes lose distinguishing power in humanized mice. Apart from differences in morphological appearance and in the expression of different levels of thermogenesis-related genes, brown and brite/beige adipose depots are also suggested to differ in expression of distinct sets of genes not directly related to thermogenesis. These genes are those that were identified in immortalized adipocytes originating from brown and brite/beige adipose depots[15,16]. Thus, they are the markers that led to the influential suggestion that, molecularly, human BAT is more equivalent to mouse brite/beige than to classical BAT[15,16,34]. To clarify the molecular identity of human BAT, it was thus necessary to validate the genes suggested to discriminate between brown and brite/beige adipose tissues in mice living under conditions approaching human conditions.

We analysed four proposed brown marker genes (*Ebf3, Eva1/Mpzl2, Fbxo31* and *Epsti1*) and four proposed brite/beige marker genes (*Cd137, Tbx1, Tmem26* and *Cited1*) (Fig. 3) (refs. [15,16]). In addition, we analysed the expression of two genes proposed to be present in both brown and brite/beige adipocytes (*P2rx5* and *Pat2*) (ref. [35]). Fully in agreement with the original observations[15,16,35], under standard housing conditions the majority of marker genes were indeed capable of discriminating between the two adipose tissues (Fig. 3a) (*Epsti1* displayed a reversed selectivity, as seen earlier[28]). However, upon humanization, the ability of essentially all suggested marker genes to distinguish between brown and brite/beige adipose tissues was considerably diminished (Fig. 3a).

To achieve an overview of the dynamic changes in marker gene expression, we performed hierarchical clustering of the selected marker genes and the two tissues under standard and physiologically humanized conditions (Fig. 3b). Clustering of the marker genes again clearly demonstrated their power to discriminate between iBAT and ingWAT in standard mice (left half of the heatmap), fully in agreement with the original observations. Importantly, brown- and brite/beige-selective genes formed two distinct clusters (top and bottom halves of the heatmap). However, each tissue responded to humanization in such a way that under humanized conditions, the tissues still clustered separately but much closer to each other (right half of the heatmap) (Fig. 3b). Thus, hierarchical cluster analysis led to the same conclusions as single-gene analysis: the selected marker genes, when considered globally, had much lower distinguishing power in physiologically humanized than standard mice.
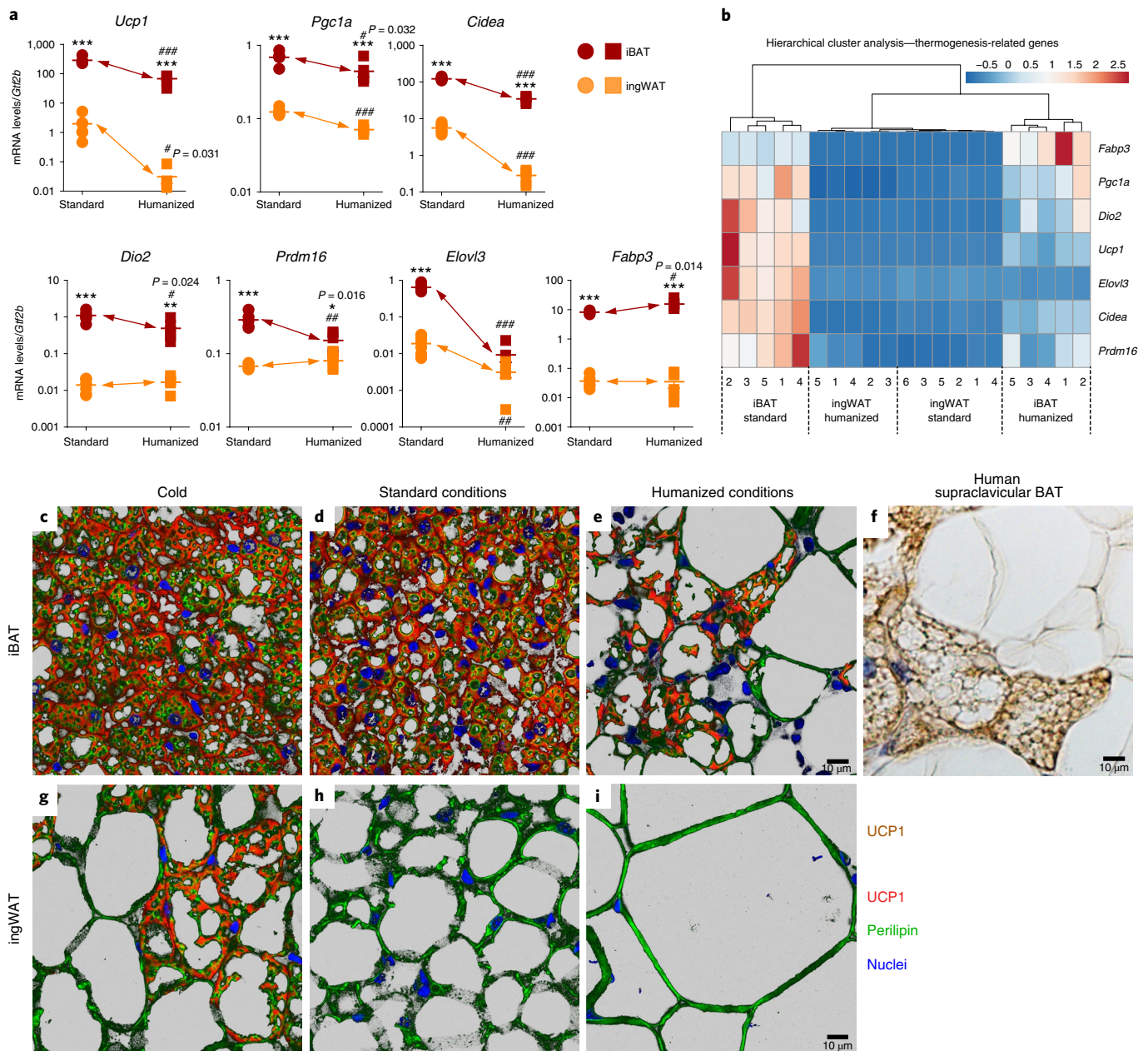
Fig. 2 | iBAT in physiologically humanized mice retains a distinct 'thermogenic' molecular signature. a,b, iBAT and ingWAT from mice exposed to standard ($n = 5$ and 6, respectively) and physiologically humanized conditions ($n = 5$) were analysed. **a,** Expression levels of brown fat-specific/enriched genes. Values are the mean ± s.e.m. Where not visible, the error bars are smaller than the symbols. The asterisks signify the significant difference between iBAT and ingWAT; *$P < 0.05$, **$P < 0.01$, ***$P < 0.001$ by two-tailed Student's *t*-test. The hash symbols indicate the significant difference between humanized and standard conditions; #$P < 0.05$, ##$P < 0.01$, ###$P < 0.001$ by two-tailed Student's *t*-test. Note the logarithmic scale. **b,** Hierarchical cluster analysis of the genes presented in **a**. The heatmap illustrates the relative gene expression. Rows are centred; unit variance scaling is applied to rows. Both rows and columns have been clustered using Euclidean distance and complete linkage. **c–e,g–i,** The animals in Fig. 1 were analysed using immunohistochemistry. **c,d,e,** Representative confocal images of iBAT stained for UCP1 (red), perilipin (green) and nuclei (blue). **g,h,i,** Representative confocal images of ingWAT stained for UCP1 (red), perilipin (green) and nuclei (blue). Scale bar, 10 μm (also applies to **c,d,g,h**). **f,** Representative image of human supraclavicular BAT stained for UCP1 (brown) and nuclei (blue). A single human supraclavicular BAT was analysed, but see earlier similar pictures[6]. Scale bar, 10 μm. **c,d,g,h,** Images are representative of at least two independent biological samples. **e,i,** Images are representative of at least five independent biological samples.

More extensive transcriptome changes in brown than in brite/beige fat upon humanization. To achieve a global view of the dynamic molecular changes upon humanization and further characterize the molecular signatures of the two tissues under the two conditions, we performed a global gene expression analysis using RNA sequencing (RNA-Seq). The analysis of transcripts differentially expressed in each of the tissues under standard and humanized conditions (Fig. 4a) extended the earlier observations: upon humanization, more than twofold more transcripts were altered in iBAT than in ingWAT (the total number of transcripts with read counts ≥ 15 was 19,685). The number of genes whose expression was regulated by humanization in a tissue-specific manner, or in both tissues, is presented in Supplementary Fig. 1.
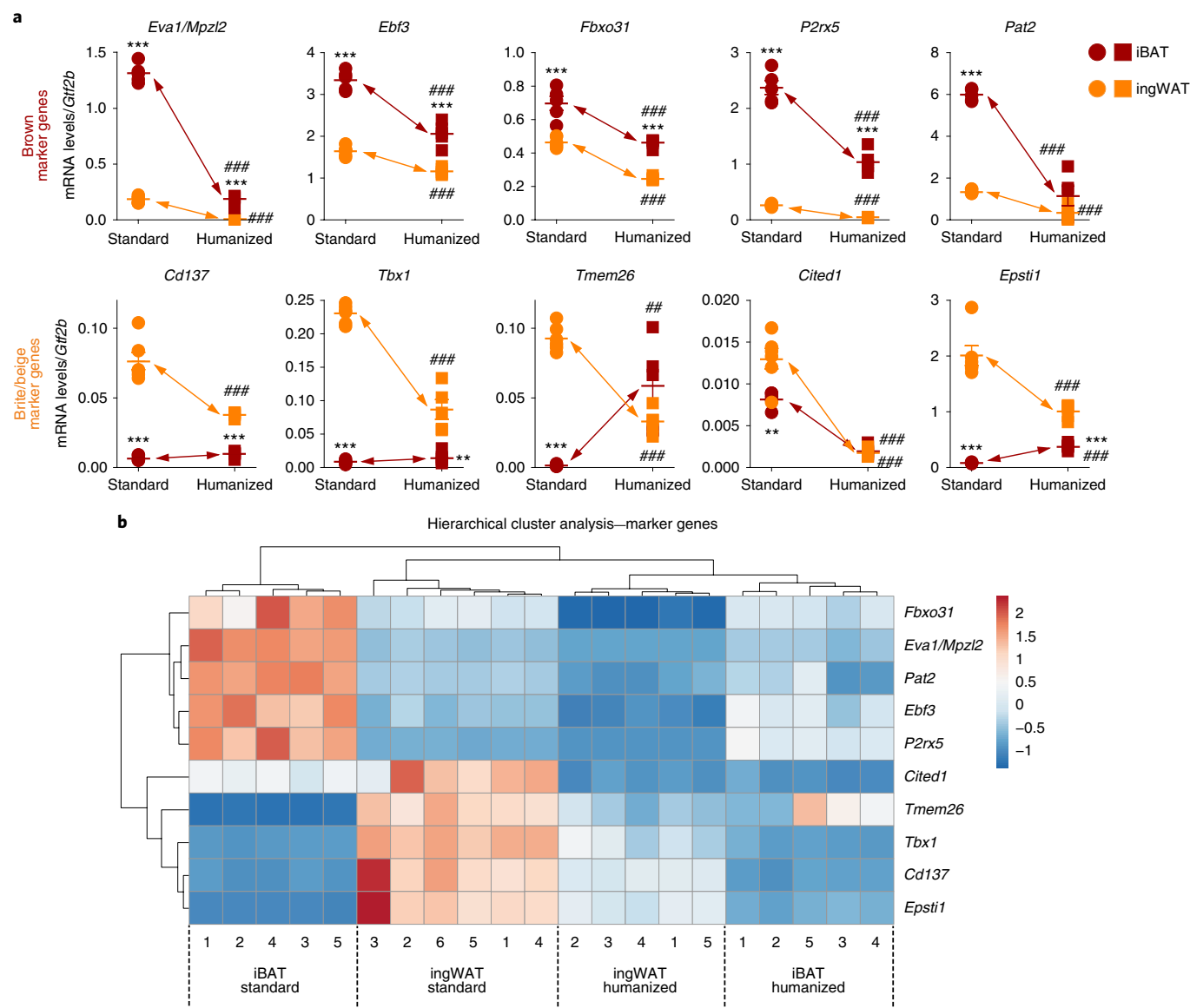
Fig. 3 | Under humanized conditions, the distinguishing power of the suggested brown versus brite/beige marker genes is diminished. The animals shown in Fig. 2a,b were analysed. **a**, Expression levels of brown (top) and brite/beige (bottom) marker genes. Values are the mean ± s.e.m. Where not visible, the error bars are smaller than the symbols. The asterisks indicate the significant difference between iBAT and ingWAT; $**P < 0.01$; $***P < 0.001$ by two-tailed, unpaired Student's t-test. The hash symbols indicate the significant difference between humanized and standard conditions; $\#\#P < 0.01$; $\#\#\#P < 0.001$ by two-tailed, unpaired Student's t-test. **b**, Hierarchical cluster analysis of the expression levels of the genes presented in **a**. The heatmap illustrates relative gene expression. Rows are centred and unit variance scaling is applied to rows. Both rows and columns are clustered using Euclidean distance and complete linkage.

Hierarchical cluster analysis of the top 1,200 expressed genes (Fig. 4b) demonstrated that the samples clustered into four groups according to tissue identity and experimental conditions. The iBAT samples from mice exposed to standard conditions formed a separate, very distinct cluster. Humanized iBAT samples were closer to ingWAT, again demonstrating the remarkable alterations occurring in brown fat upon humanization.

To compare humanization-dependent transcriptional changes globally, we performed principal component analysis (PCA) of the entire iBAT and ingWAT transcriptomes under standard and physiologically humanized conditions (Fig. 4c). The samples assembled into four groups. The transcriptomes of standard and humanized ingWAT were very similar. In contrast, standard and humanized iBAT were markedly separated, the latter taking on a profile more similar to that of ingWAT. Thus, humanization led to marked general

transcriptome remodelling in classical brown and to a much lesser extent in brite/beige adipose tissue. Noteworthy, brown and brite/beige adipocytes, as recently reported, also display great differences in epigenomic plasticity: in response to thermoneutrality, after prior exposure to strong cold, chromatin in brite/beige, but not in brown adipocytes, undergoes dramatic remodelling[22].

The transcripts from nonadipose cells in the tissues contribute to the global adipose tissue transcriptomes analysed in this study and thus represent a confounding factor when studying the expression profiles of adipocytes as such. To circumvent this limitation, we took advantage of the availability of a set of 119 genes identified in a recent study, which compared the transcriptomes of pure brown, brite/beige and white adipocytes with the transcriptomes of complex adipose tissue biopsies[36]. These so-called 'BATLAS' genes thus represent true adipocyte genes. The expression of
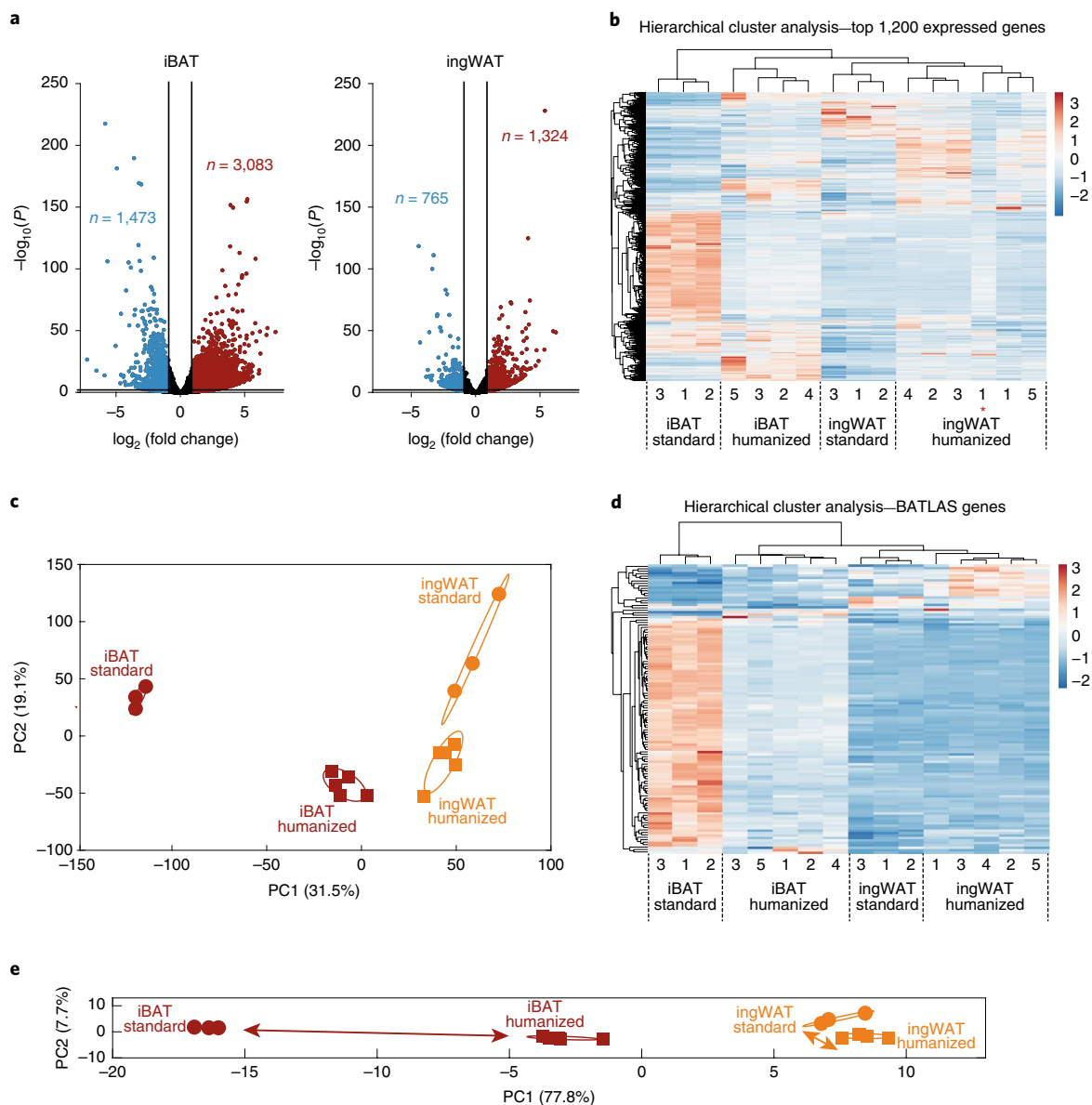
Fig. 4 | Physiological humanization leads to more extensive transcriptome alterations in iBAT than in ingWAT. A subset of the animals presented in Figs. 2a,b and 3 was analysed. The transcriptomes of iBAT and ingWAT from physiologically humanized mice ($n = 5$) and mice exposed to standard conditions ($n = 3$) were analysed using RNA-Seq. **a**, Volcano plot demonstrating differences in gene expression between humanized and standard conditions. The $\log_2$ gene expression ratios (fold change) are plotted against negative $\log_{10} P$ values. The negative $\log_{10}P < 0.05$ cut-off is indicated by the horizontal line. The ≥ 2 and ≤ -2 fold change cut-offs are indicated by the vertical lines. Differentially expressed genes were identified using the DESeq2 algorithm, implementing a negative binomial distribution and a generalized linear model statistical test. **b**, Hierarchical cluster analysis of the top 1,200 expressed genes. The heatmap illustrates relative gene expression. Rows are centred and unit variance scaling is applied to rows. Both rows and columns are clustered using Euclidean distance and complete linkage. One outlier on the right side of the heatmap (iBAT-humanized1) is marked with an asterisk. **c**, PCA of the whole transcriptomes of the indicated samples. Each symbol represents one sample. The numbers in parentheses on the axes represent the proportion of data variance explained by each principal component. Note that to obtain uniform representation of variance over the graph surface, the axes were adjusted according to the percentage of variance explained by each of the components. **d**, Hierarchical cluster analysis of the expression levels of the BATLAS genes. The heatmap illustrates relative gene expression. Rows are centred and unit variance scaling is applied to rows. Both rows and columns are clustered using Euclidean distance and complete linkage. **e**, PCA of the BATLAS genes. Each symbol represents one sample. The numbers in parentheses on the axes represent the proportion of data variance explained by each principal component.

BATLAS genes in the iBAT and ingWAT of standard and humanized mice was visualized as a heatmap on the basis of hierarchical clustering (Fig. 4d). An even more distinct clustering of standard iBAT samples was observed. Humanized iBAT samples formed a separate cluster that, consistently with the previous hierarchical cluster analyses (Figs. 2b, 3b and 4b), was closer to ingWAT than to standard iBAT samples.

The consequences of humanization on the expression of BATLAS genes in each of the adipose depots were also visualized with PCA (Fig. 4e). All samples separated into four different groups determined by origin and experimental conditions. The effect of humanization in ingWAT was rather small. In contrast, the two iBAT groups were clearly separated: the humanized iBAT group was different from the standard iBAT, but also clearly distinct

from ingWAT, demonstrating that the tissue had attained a unique molecular signature.

Thus, analysis of both the entire transcriptomes and genes that define adipose cells (BATLAS genes) fully verified that humanization caused significant molecular changes in classical brown fat. Changes in the brite/beige adipose depot were of much lower magnitude.

Humanized mouse iBAT molecularly phenocopies human supraclavicular BAT. The gene expression profiles of mouse classical brown and brite/beige adipose tissues characterized in this study enabled us to explore the molecular identity of human BAT (that is, as classical brown or brite/beige) by using comparative transcriptomics. The transcriptomes of a series of human brown, as well as of human white, fat biopsies have recently been profiled using RNA-Seq[36]. These fat biopsies (verified functionally as brown or white) were obtained from the supraclavicular region of healthy individuals[36].

We first attempted a global approach by comparing the entire transcriptomes of mouse and human adipose tissues (Supplementary Fig. 2). However, in the resulting PCA, the human and mouse samples were clustered by species rather than by tissue identity (Supplementary Fig. 2a). This outcome was not surprising given that for many tissues, global gene expression profiles are more similar among different tissues within a species than between corresponding tissues of two species[37]. As recently elaborated[38], when considered globally, transcriptomes cluster preferentially according to the organ or according to the species as a consequence of the dominant behaviour of 'tissue-variable' or 'species-variable' genes, respectively. Organs with distinct signatures of tissue-specific (tissue-variable) genes, such as brain, testis, heart, liver and kidney, show strong organ-dependent clustering[37,39–41]. Importantly, adipose tissue is among the tissues that express the lowest number of tissue-specific (tissue-variable) genes[37] and therefore demonstrates strong species-dependent clustering (Supplementary Fig. 2a and refs. [37,38]). Species-dominated clustering can be significantly reduced when PCA is performed on a subset of transcripts varying preferentially across organs[38]. Therefore, instead of using a global approach, we restricted our analysis to a subset of genes with strong adipose tissues signatures.

The brown versus brite/beige marker genes were originally identified as showing distinct expression levels across various adipose tissues in mice[15,28] and humans[15,16,35] (see also Supplementary Fig. 3b). However, analysis of their expression levels in an extensive set of brite/beige and brown adipose depots, in cultured adipocytes originating from conventional brite/beige and brown adipose tissues[28], and in the relevant adipose depots of mice exposed to various physiological conditions (this study; Fig. 3), as well as cell type-specific gene expression profiling[22], failed to demonstrate the expected tissue and cell type specificity of the suggested brown versus brite/beige marker genes. Nonetheless, since these marker genes under some experimental conditions (for example, standard housing conditions; Fig. 3) were competent in discriminating between the conventional brown (iBAT) and brite/beige (ingWAT) adipose depots, we performed PCA using these genes to reveal the relationships between human BAT and WAT and the two mouse tissues under three conditions—humanized, standard and cold (acclimation to 4 °C; Fig. 5a). Due to stringent data preprocessing, *P2rx5* and *Cited1* had to be omitted from the analysis; two recently identified brown marker genes, *Slc29a1* and *Hoxa5*[22], were included instead. Based on the expression of these marker genes, the mouse humanized iBAT samples were positioned closest to the human BAT samples (Fig. 5a), again demonstrating similarity between mouse classical BAT and human BAT. The fact that the mouse cold ingWAT samples were equally close to human BAT and standard ingWAT was the second closest group in similarity to human BAT rationalizes the previous conclusions that human BAT is composed of brite/beige adipocytes, a conclusion that is thus

fully valid under the conditions originally employed[15,16,34]. Indeed, in the PCA, iBAT samples from standard mice were well separated from human BAT, as was originally concluded (Fig. 5a, brown circles). Fully thermogenically recruited mouse iBAT samples (from mice acclimated to 4 °C) were even more distant from the human BAT samples than the standard mouse iBAT samples (Fig. 5a, dark blue snowflakes).

Thus, using the marker genes that, when originally analysed, indicated a close relationship between mouse brite/beige adipose tissue and human BAT, when reanalysed with physiologically more relevant mouse samples, led to the conclusion that mouse classical BAT and human BAT were the most closely associated tissues.

The BATLAS genes, selected for their adipose-selective expression[36], also fulfill the criteria for being clustered in an organ-dominated manner. The PCA of human BAT and WAT versus the two mouse tissues under the three conditions demonstrated very clear tissue-dominated clustering (Fig. 5b). Importantly, mouse humanized iBAT and human BAT were positioned close to each other, as were mouse humanized ingWAT and human WAT. In agreement with Fig. 4e, mouse standard iBAT formed a distinct cluster positioned far from the other samples. Also for this gene collection, the BAT of mice acclimated to 4 °C showed a molecular profile even more distant from human BAT, whereas the corresponding ingWAT was almost indistinguishable from the classical BAT of physiologically humanized mice.

Thus, the BATLAS genes demonstrated notable power in discriminating between brown, brite/beige and white adipose tissues. Importantly, the molecular signature of human BAT, when compared to the molecular signatures of classical brown and brite/beige adipose tissues of the mice studied under conditions relevant to human physiology, displayed similarity only to classical BAT.

To examine the generality of these findings, an additional brown fat depot—from the human perirenal region–was included in the analysis. Analysed biopsies were taken from the upper kidney pole and were selected based on their multilocular appearance[42]. As can be seen in the PCA plots for the marker and BATLAS genes (Supplementary Fig. 4), the samples of human perirenal BAT formed separate clusters that were positioned close to the human supraclavicular BAT samples. Thus, human perirenal and supraclavicular brown fat display similar molecular characteristics; therefore, it may be suggested that the classical BAT of physiologically humanized mice presumably phenocopies human BAT in general.

UCP1 is the most central thermogenic protein; therefore, we examined specifically the expression levels of *Ucp1* in human and mouse adipose tissues. The expression levels of *Ucp1* in mouse brite/beige adipose tissue are about 100-fold lower than in classical BAT, both under standard and humanized conditions (for example, see Fig. 2a) and about tenfold lower under cold conditions[25]. We calculated the *Ucp1* messenger RNA levels directly from the RNA-Seq data of the mouse and human samples using general transcription initiation factor IIB (*Gtf2b*) as a reference gene, analogously to quantitative PCR analysis (for details, see Supplementary Fig. 4). The difference in *Ucp1* expression levels between mouse brown and brite/beige adipose tissues was maintained (as expected) (Fig. 5c and Supplementary Fig. 4c). Importantly, the human brown fat *UCP1/GTF2B* mRNA levels were practically identical to those observed in humanized mouse iBAT. Thus, human BAT and humanized mouse BAT are very similar in their actual thermogenic potential, which is about 100-fold higher than in the corresponding brite/beige adipose tissues.

Apart from demonstrating distinct gene expression signatures, mouse classical brown and brite/beige adipose depots also greatly differ in chromatin structure[22]. Future comparative epigenomic studies, aimed at revealing the chromatin signatures of human brown fat and classical brown and brite/beige adipose tissues in physiologically humanized (and standard) mice, may further clarify the molecular identity of human brown fat.
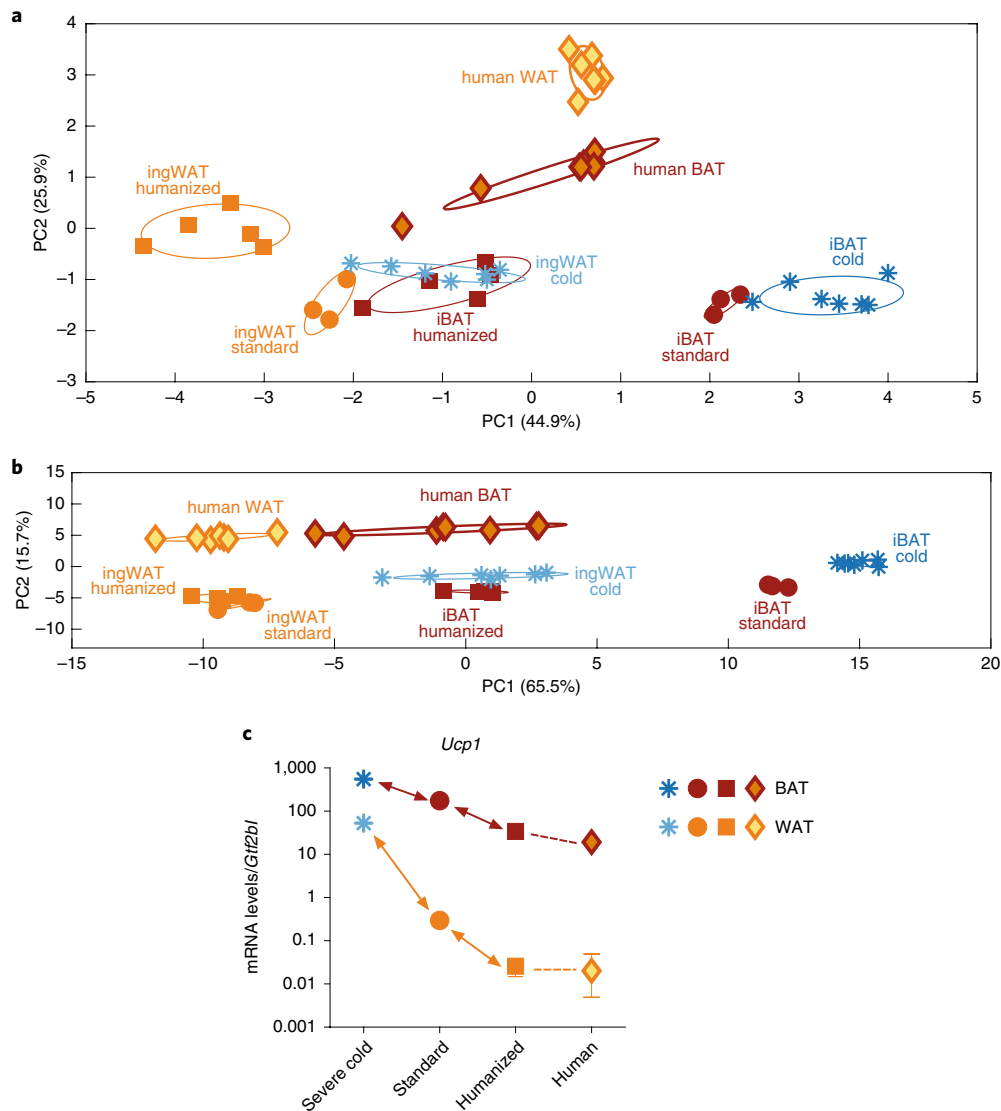
Fig. 5 | iBAT in physiologically humanized mice molecularly phenocopies human supraclavicular BAT. The human BAT ($n=8$) and WAT ($n=7$) from the supraclavicular region and iBAT and ingWAT from physiologically humanized and standard mice (shown in Fig. 4), as well as iBAT and ingWAT from mice acclimated to severe cold ($n=7$), were analysed using RNA-Seq. **a**, PCA of marker genes (brown: *Fbxo31*, *Eva1/Mpzl2*, *Pat2*, *Ebf3*, *Slc29a1*, *Hoxa5*; brite/beige: *Tmem26*, *Tbx1*, *Cd137*, *Epsti1*). Each symbol represents one sample. The numbers in parentheses on the axes represent the proportion of data variance explained by each principal component. Note that to obtain uniform representation of variance over the graph surface, the axes were adjusted according to the percentage of variance explained by each of the components. **b**, PCA of the BATLAS genes. Each symbol represents one sample. The numbers in parentheses on the axes represent the proportion of data variance explained by each principal component. Note that to obtain uniform representation of variance over the graph surface, the axes were adjusted according to the percentage of variance explained by each of the components. **c**, Expression levels of *Ucp1* in mouse and human adipose tissues (shown in Figs. 4 and 5a,b) normalized per *Gtf2b* expression. *Ucp1* and *Gtf2b* expression levels were determined with RNA-Seq. Values are the mean ± s.e.m. Where not visible, the error bars are smaller than the symbols. Note the logarithmic scale.

Humanized iBAT and human BAT retain high browning potential. The significantly lower levels of mRNA for thermogenesis-related proteins in the BAT of physiologically humanized mice compared to the BAT of mice living under subthermoneutral conditions (Figs. 2a,b and 5c) strongly indicated that the thermogenic capacity of the tissue was also markedly diminished (for example, see refs. [25,43]). Thus, it is of considerable physiological and translational importance to determine whether the tissue, upon adequate stimulation, could (re)gain a high thermogenic capacity and thus (re)gain the ability to combat or counteract obesity. The demonstration of such an ability would suggest that human BAT should possess a similar potential for recruitment. The computational tool PROFAT (http://profat.genzentrum.lmu.de) can be used to predict the browning probability of both mouse and

human adipose tissues by identifying the unbiased and robust gene signatures of brown and white adipocytes[44]. We exploited PROFAT to analyse the gene expression datasets from both mouse and human adipose tissues. The analysis resulted in the prediction that all mouse classical BAT samples, as well as nearly all human BAT samples (6 out of 8), could, with almost 100% probability, acquire the phenotype of thermogenically active BAT (Fig. 6a). Notably, none of the brite/beige samples was predicted to exhibit high browning probability.

Furthermore, PROFAT-based hierarchical clustering classified all mouse iBAT samples (Supplementary Fig. 5) and 6 out of 8 human BAT samples (Supplementary Fig. 6) as brown. Importantly, the predicted browning probability was not directly correlated with the actual 'brownness' of the examined tissues. This conclusion was
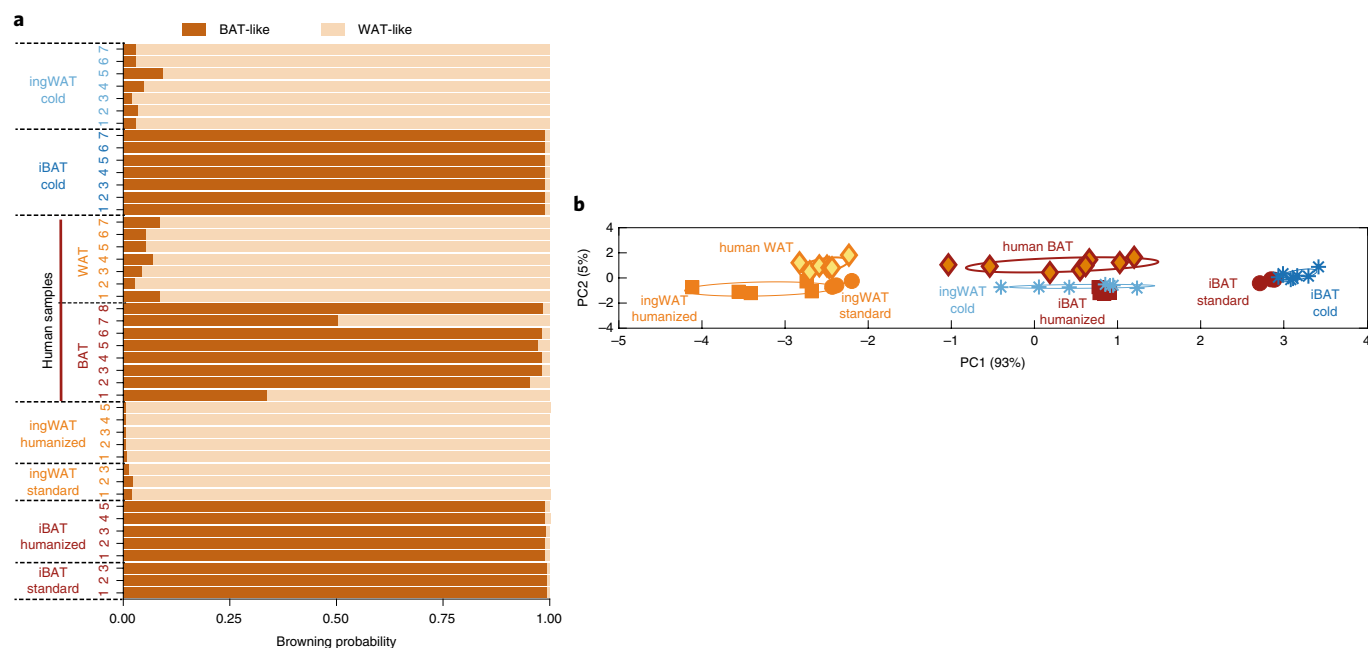
Fig. 6 | Browning probability in human and mouse adipose tissues. a, The browning probability of all samples analysed in Fig. 5 was predicted using the computational tool PROFAT. **b**, PCA of the thermogenesis-related genes (*Ucp1, Pgc1a, Cidea, Dio2, Prdm16, Elovl3 and Fabp3*) in all samples analysed in Fig. 5. Each symbol represents one sample. The numbers in parentheses on the axes represent the proportion of data variance explained by each principal component. Note that to obtain uniform representation of variance over the graph surface, the axes were adjusted according to the percentage of variance explained by each of the components.

based on the PCA of the thermogenesis-related genes (Fig. 6b) (the same genes as in Fig. 2a,b). This analysis permitted a global view of the actual thermogenic capacities—brownness—of all adipose samples examined. Although human BAT, mouse humanized iBAT and mouse cold ingWAT displayed almost identical brownness (Fig. 6b), only human BAT and humanized iBAT were predicted, by PROFAT, to be competent to acquire high thermogenic capacity (Fig. 6a). Thus, the molecular signatures identified by the PROFAT analysis also strongly suggest that human BAT is more similar to classical brown than to brite/beige tissue.

To experimentally verify this prediction, we acclimated a group of physiologically humanized mice to regular cold (4 °C), a physiological condition that leads to both recruitment of brown fat thermogenic capacity and activation of thermogenesis in the tissue[45]. As can be seen in Fig. 7b, upon cold acclimation, the BAT of physiologically humanized mice developed distinctive histological and cellular characteristics: the majority of adipocytes were multilocular and UCP1+ and the protein concentration was significantly higher than in the BAT of humanized mice (Fig. 7h). Thus, acquisition of a higher thermogenic capacity was unambiguously verified.

Immunohistochemical analysis of ingWAT from physiologically humanized mice subsequently acclimated to cold (Fig. 7e) again fully verified the PROFAT prediction: the majority of adipocytes were unilocular and UCP1−. Only occasional adipocytes were multilocular but were still UCP1−. The tissue was principally morphologically very similar to the ingWAT of physiologically humanized mice (Fig. 7d) and notably different from the tissue in mice acclimated to cold in the conventional way, which is rich in multilocular UCP1+ adipocytes (Fig. 7f).

The total amount of UCP1 in the tissue is generally accepted to be the most relevant biochemical parameter to predict the nonshivering thermogenic capacity of thermogenesis-competent adipose tissues[45,46]. In agreement with the immunohistochemical observations, the immunoblot analysis demonstrated that UCP1 protein

levels in the BAT of physiologically humanized mice subsequently acclimated to cold were significantly increased in comparison to the levels in the BAT of humanized mice (Fig. 7g, left part of the immunoblot and Supplementary Fig. 7). Importantly, UCP1 was not detected in the ingWAT of either physiologically humanized mice (as expected) or cold-acclimated, previously physiologically humanized mice (Fig. 7g, right part of the immunoblot). Based on the data presented in Supplementary Fig. 7 (UCP1 protein levels expressed per mg protein) and Fig. 7i (total protein content in the tissue), we calculated the total UCP1 levels in all the tissues (Fig. 7j). Notably, total UCP1, that is, the nonshivering thermogenic capacity of BAT in physiologically humanized mice subsequently acclimated to cold was nearly 30-fold higher than in the BAT of humanized mice kept at 30 °C. Thus, the PROFAT-predicted browning of nearly 100% probability was fully verified. Importantly, the only thermogenically competent adipose tissue in humanized mice was the classical BAT; upon cold acclimation, the brite/beige adipose tissue of humanized mice did not acquire any thermogenic capacity.

The thermogenic competence of brite/beige fat is abrogated mainly by age. Since the browning competence of brite/beige adipose depots was largely influenced by the previous history of the animal, we examined which of the factors—nutritional, thermal and/or age—was the most influential. We first examined the effects of diet. As seen in Supplementary Fig. 8, the brite/beige depots of only thermally (but not nutritionally) humanized mice could not undergo browning upon prolonged exposure to cold. Thus, an energy-rich diet was not the main factor that caused the inhibition of brite/beige adipose tissue browning in physiologically humanized mice.

Very prolonged exposure to thermoneutrality could hypothetically influence sympathetic innervation in brite/beige adipose depots in such a way that the tissue would not be sufficiently adrenergically stimulated upon exposure to cold. Therefore, to enforce stimulation of all adipose depots, we treated thermally humanized mice with
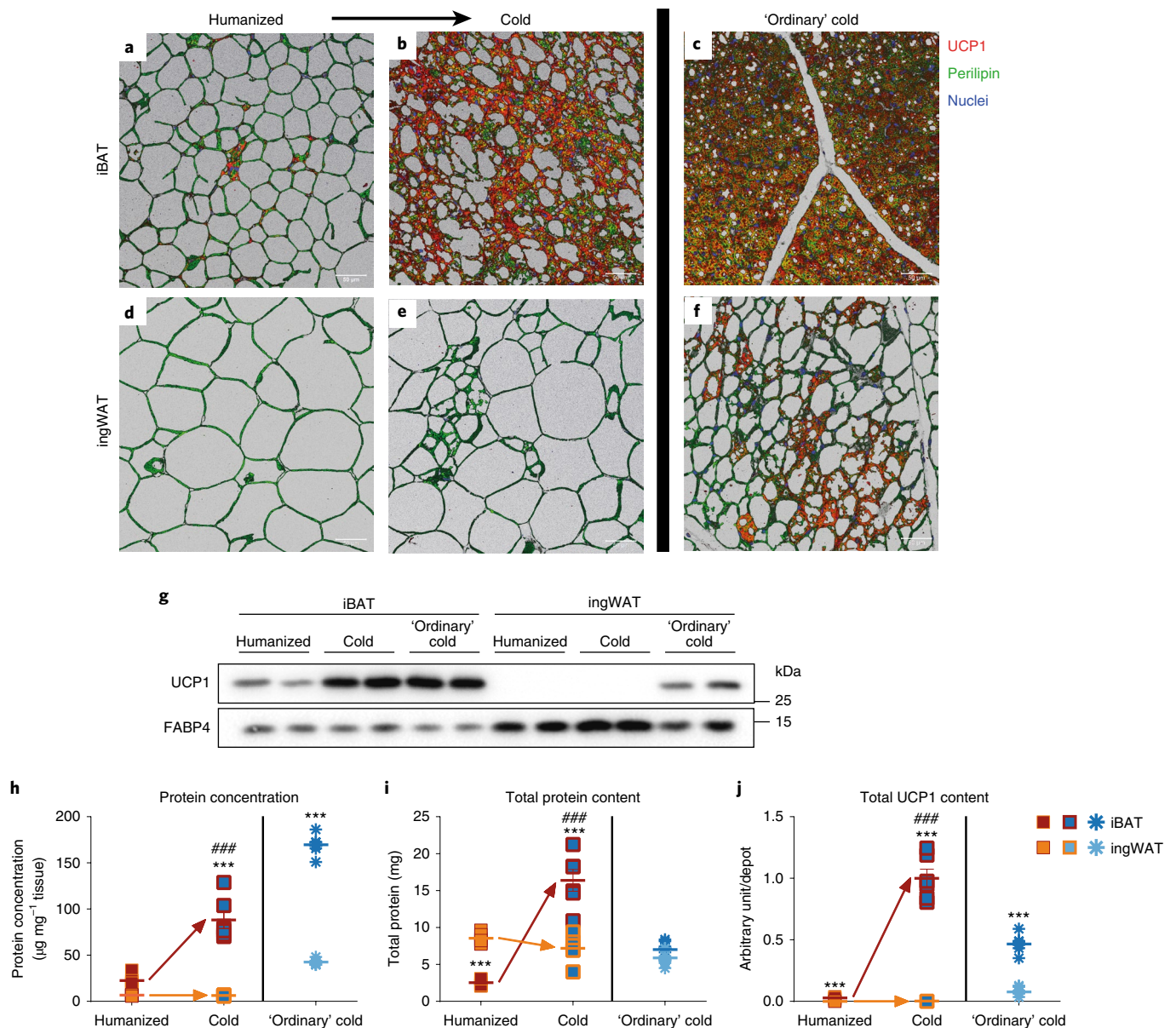
Fig. 7 | Physiologically humanized mouse iBAT, but not ingWAT, retains high browning capacity. After being physiologically humanized, C57BL/6N mice were either acclimated to a temperature of 4 °C or were killed (control physiologically humanized mice). C57BL/6N mice acclimated to a temperature of 4 °C in the conventional way are those presented in Fig. 2c,g. **a**–**f**, Representative confocal images of iBAT (**a,b,c**) and ingWAT (**d,e,f**) stained for UCP1 (red), perilipin (green) and nuclei (blue) using immunohistochemistry. Scale bar, 50 μm. **a,b,d,e**, Images are representative of four independent biological samples. **c,f**, Images are representative of at least two independent biological samples. **g**, Representative immunoblots of UCP1 and FABP4 in the iBAT and ingWAT of the mice shown in **a**–**f**. **h**–**j**, Protein concentration (**h**) and total protein content (**i**) in one lobe/pad of the iBAT and ingWAT of the mice shown in **a**–**f** (physiologically humanized ($n=6$); cold-acclimated, previously physiologically humanized ($n=6$); cold-acclimated in the conventional way ($n=7$)). Values are the mean ± s.e.m. Where not visible, the error bars are smaller than the symbols. The asterisks indicate the significant difference between iBAT and ingWAT; $P < 0.001$ by two-tailed, unpaired Student's t-test. The hash symbols indicate the significant difference between humanized and cold conditions; $P < 0.001$ by two-tailed, unpaired Student's t-test. **j**, Total UCP1 content in the iBAT and ingWAT of the mice in **c**–**h**. The total UCP1 content in the iBAT of physiologically humanized, cold-acclimated mice was set to 1.0; the levels in the ingWAT and iBAT of physiologically humanized mice and mice acclimated to 4 °C in the conventional way were expressed relative to this value. Values are the mean ± s.e.m. Where not visible, the error bars are smaller than the symbols.

the potent β₃-adrenergic receptor-selective agonist CL 316,243 for 3 weeks. This strong pharmacologically mediated adrenergic stimulation could not induce browning in ingWAT (Supplementary Fig. 9). Thus, an insufficient sympathetic stimulation could not explain the inability of brite/beige adipose depots of physiologically humanized mice to undergo browning upon acclimation to cold.

To examine whether very prolonged exposure to thermoneutrality was the reason for the inability of ingWAT to brown upon exposure to 4 °C, mice that were of similar age to thermally humanized mice (8 month old), but were raised and maintained under standard conditions (21 °C), were exposed to the same cold regime (as stated earlier). As shown in Supplementary Fig. 10, ingWAT (but not iBAT) failed to brown in response to cold stimulation also in these mice. Thus, neither nutritional nor thermal conditions could explain the observed feature of browning incompetence in ingWAT.

The fact that physiologically humanized mice were about 9 months old when exposed to cold (as opposed to 2 months in the conventional cold acclimation experiments), strongly suggests that age is the factor that determines the inability of brite/beige adipose tissue to undergo browning upon acclimation to cold (in agreement with Berry et al.[47]). To corroborate these findings, we initiated cell cultures with adipose precursors originating from classical brown and brite/beige depots of young (4 weeks) and old (8 months) mice. To mimic the continuous sympathetic stimulation occurring upon cold exposure, cells were continuously treated (or not) with noradrenaline. As shown in Supplementary Fig. 11, brown preadipocytes originating from the classical brown fat of old mice displayed adipogenic and thermogenic capacities similar to the brown preadipocytes originating from young mice. In contrast, in adipocyte cultures originating from the brite/beige adipose depot of old mice, *Ucp1* mRNA could not be induced upon chronic treatment with noradrenaline (Supplementary Fig. 12); their adipogenic capacity was also diminished. Therefore, based on both in vivo and in vitro experiments, it may be concluded that age is the factor mediating abrogation of the thermogenic competence of brite/beige, but not classical BAT, depots.

Discussion

In the present study, we demonstrate that general observations regarding the principal advantage of using physiologically humanized mice for translationally focused research extends to issues concerning the nature and function of adipose tissues. Thus, whereas data from young adult mice reared and maintained under standard animal house conditions—mild cold stress and uninteresting food–indicated a similarity between human BAT and mouse brite/beige adipose tissues, this association was radically altered when the analysis was performed with physiologically humanized mice. If middle-aged mice are maintained under conditions approaching human thermal and nutritional conditions, human BAT has its closest parallel in mouse classical BAT. Analysis of recently identified brown fat depots in mice (for example, supraclavicular depots) indicates that mouse fat depots also demonstrate a high degree of anatomical similarity to those in humans[48].

The suggestion that mouse brite/beige adipose tissues are more closely related to human BAT than is mouse classical BAT[15,16] has resulted in considerable attention being directed towards brite/beige adipose tissues in translationally focused studies (as discussed in, for example, refs. [8,31,49–51]). In young adult mice, ingWAT can acquire significant thermogenic capacity (in cold-acclimated mice approximately 20% of nonshivering thermogenesis could be performed in brite/beige depots; Fig. 6h,l and, for example, refs. [25,28,32,33,43]). However, in middle-aged mice, cold and chronic β_3-adrenergic stimulation were totally ineffective in inducing browning of the brite/beige adipose depot while thermogenic competence in classical BAT was fully preserved. This complete absence of thermogenic competence in the humanized brite/beige adipose depots strongly suggests that enhancement of a heat-producing and thus lipid-consuming capacity of certain WAT depots in humans is unlikely to arise through physiological or pharmacological means (although there may be exceptions[52]). In contrast, fully preserved thermogenic competence of classical BAT implies that in humans exposed to analogous physiological or pharmacological stimuli, classical BAT depots would be capable of being recruited and transformed into tissue with high thermogenic activity. As reported in previous studies, in humans acclimated to mild cold, moderate brown fat recruitment was observed[53–55]. However, the existing literature on brown fat-related tumours in humans (pheochromocytoma and hibernoma)[56–60] indicates that human brown fat has the potential to achieve remarkably high recruitment states. Therefore, translational efforts directed towards the highly recruitable classical BAT of mice would probably have a considerable possibility of resulting in clinically relevant outcomes.

Methods

Human samples. For morphological examination, supraclavicular fat was collected during cadaveric examination. The source was a 21-year-old (healthy) male with a body mass index of 22. The study protocol was approved by the Ethics Committee of the University of Ancona. Formal consent was obtained from the relatives. This specific sample was collected from the collarbone area, not very deep and not in close relationship with the large blood vessels present in this region.

For RNA-Seq, human supraclavicular BAT and WAT biopsies were obtained from the supraclavicular region of healthy individuals using the positron emission tomography/computed tomography-guided procedure described in Orava et al.[61] and were those investigated by Perdikari et al.[36]. The study protocol was approved by the Ethics Committee of the Hospital District of Southwest Finland and conducted according to the principles of the Declaration of Helsinki (edition based on the WMA General Assembly, Tokyo 2004). All study participants provided written consent before entering the study. The site of the biopsy was decided by the cold exposure fludeoxyglucose-positron emission tomography/computed tomography image that showed activated BAT. A subcutaneous WAT sample was collected from the same incision. The biopsies were obtained under local lidocaine with adrenaline anaesthesia by a plastic surgeon at normal room temperature (20 °C). Immediately after removal, tissue samples were snap-frozen in liquid nitrogen. Perirenal adipose tissue biopsies were collected during nephrectomy and were those investigated by Jespersen et al.[42]. Only samples from the upper kidney pole were included in the analysis.

Animal samples. All experiments were approved by the Animal Ethics Committee of the North Stockholm Region. The experiments were performed on mice exposed to different physiological conditions (described later in the Methods). All groups had free access to water and food and a 12:12-h light–dark cycle regime. Unless otherwise stated, mice had access to a chow diet (R-70; Lactamin). Mice were randomly assigned to treatment groups. The analysis of samples from different physiological conditions was performed in parallel, as indicated in the corresponding experiments.

For analysis under standard conditions, C57BL/6N male mice were bought from the Charles River Laboratories and kept at 21 °C until 8 weeks of age.

To analyse the effects of conventional cold acclimation, samples in this study were obtained from male C57BL/6N mice purchased from the Charles River Laboratories or bred at the institute and described in Fischer et al.[25]. At the start of the experiment, 8-week-old C57BL/6N male mice were single-caged and successively acclimated to cold by first placing them at 18 °C for 1 week and then at 4 °C for the following 4 weeks[62].

To analyse the effects of physiologically humanized conditions, the samples analysed in this study were from the wild-type mice (mixed C57BL/6N and C57BL/6J substrain background) bred at the institute, described and metabolically characterized in Abreu-Vieira et al.[27]. Before the start of the experiment, mice were housed at 22–24 °C. At the start of the experiment, 12-week-old male mice were single-caged and transferred to 30 °C (thermoneutrality). Mice had access only to a high-fat diet (45% calories from fat; D12451; Research Diets). Mice were kept at thermoneutrality for at least 25 weeks.

To study cold acclimation after physiological humanization, 12-week-old C57BL/6N male mice (purchased from the Charles River Laboratories) were transferred to 30 °C (thermoneutrality, 4 mice per cage). Mice had access only to a high-fat diet (45% calories from fat, D12451 diet) during the first 22 weeks of humanization, and to the compositionally identical 245HF diet (SAFE) until the end of the experiment (the supplier was switched due to European Union regulations). After 26 weeks at thermoneutrality and on a high-fat diet, half of these physiologically humanized mice were euthanized (control group, physiologically humanized—not cold exposed). The other half of these physiologically humanized mice were single-caged and successively acclimated to cold by first placing them at 18 °C for 1 week and then at 4 °C for the following 6 weeks. During cold acclimation, mice remained on the high-fat diet (245HF).

Sampling of animal tissues. Animals were sacrificed using CO_2 anaesthesia. iBAT and ingWAT were quantitatively dissected.

The left and right lobes were placed in separate tubes and were either directly snap-frozen in liquid nitrogen and stored at −80 °C or fixed in formaldehyde solution for histological analysis.

Morphological analysis of adipose tissues. Immunohistochemistry of human samples was performed on 3-μm-thick paraffin-embedded sections. After dewaxing, sections were thoroughly rinsed in PBS, reacted with 0.3% H_2O_2 (in PBS; 30 min) to block endogenous peroxidase, rinsed again with PBS and incubated in a 3% blocking solution (in PBS; 60 min). They were then incubated with the primary antibody against UCP1 (in PBS, overnight at 4 °C). UCP1 was localized using a rabbit polyclonal antibody against a synthetic peptide conjugated to keyhole limpet haemocyanin, corresponding to amino acids 145–159 of human UCP1, with an N-terminal cysteine added (catalogue no. ab10983; Abcam). After a thorough rinse in PBS, sections were incubated in a 1:200 v/v biotinylated secondary antibody solution (in PBS, 30 min; (Sigma-Aldrich). The biotinylated secondary antibody (Vector Laboratories) was a goat anti-rabbit immunoglobulin

G (IgG) antibody. Histochemical reactions were performed with the Vectastain ABC HRP Kit (catalogue no. BP-9100; Vector Laboratories) and SIGMA*FAST* 3,3′-diaminobenzidine as the substrate (Sigma-Aldrich). Finally, sections were counterstained with haematoxylin, dehydrated and mounted in Entellan (Sigma-Aldrich). Staining was never observed when the primary antibody was omitted.

Mouse adipose tissue depots were immersion-fixed in 4% formaldehyde (4% formaldehyde in ethanol) for 24 h, then dehydrated and embedded in paraffin using a standard procedure[63]. Tissues were sectioned using a standard microtome (RM2255; Leica Microsystems); 5-µm-thick sections were mounted on SuperFrost Plus Adhesion slides (VWR International), then deparaffinized, rehydrated and stained with haematoxylin and eosin.

Immunohistochemistry was performed on paraffin slides. To unmask antigenicity, deparaffinized and rehydrated slides were boiled in citrate buffer (10 mM sodium citrate, pH 6) in a water bath for 30 min and cooled on the bench top for 30 min. Sections were then incubated in 0.3% Sudan Black B (catalogue no. 199664; Sigma-Aldrich) in 70% ethanol for 30 min at room temperature to block autofluorescence. Slides were rinsed with PBS and then placed in a humid chamber for incubation with blocking solution (3% BSA in PBS) for 2 h at room temperature. Negative controls were run to detect autofluorescence and any nonspecific binding. Primary antibodies were diluted in 1% BSA in PBS and a volume of 50–100 µl was pipetted on each tissue section for 24 h incubation at 4 °C in a humid chamber. Primary antibody dilutions were 1:250 for the anti-perilipin-1 antibody (catalogue no. ab61682; Abcam) and 1:500 for the anti-mouse UCP1 antibody (rabbit polyclonal, raised against the C-terminal decapeptide; not commercially available). After primary antibody incubation, slides were washed with PBS for 1 h and then incubated with secondary antibodies (chicken anti-rabbit IgG cross-adsorbed secondary antibody Alexa Fluor 488; catalogue no. A21441; Molecular Probes) at a 1:500 dilution for 1 h and donkey anti-goat IgG (H+L) cross-adsorbed secondary antibody, Alexa Fluor 594 (catalogue no. A11058; Molecular Probes) at a 1:250 dilution for 1 h. After secondary antibody incubation, sections were washed with PBS for 1 h. To stain the nuclei, sections were incubated in 1 µg ml^{-1} Hoechst 33258 (catalogue no. 861405; Sigma-Aldrich) for 10 min, washed with PBS for 30 min and mounted with ProLong Gold Antifade Mountant (catalogue no. P36934; Invitrogen). Slides were kept in the dark after secondary antibody incubation. Sections were analysed with a confocal LSM 780 microscope (ZEISS). For clarity, UCP1 is shown in red, perilipin in green and nuclei in blue.

Cell culture. Primary cultures of brown and brite/beige adipocytes were prepared from BAT (combined interscapular, cervical and axillary depots) and ingWAT, respectively. The tissues of 1-month or 8-month-old C57Bl/6N mice were dissected and prepared for cell culture as described in Petrovic et al.[64]. Cells were continuously treated (or not) with 1 µM noradrenaline (catalogue no. A9512; Sigma-Aldrich). On day 7, cells were collected in TRI Reagent (catalogue no. T9424; Sigma-Aldrich) and kept at −80 °C until RNA isolation.

RNA analysis. RNA from human samples was isolated as described in Perdikari et al.[36]. Total RNA from mouse samples was extracted from frozen adipose tissue (left lobe/pad) with TRI Reagent according to the manufacturer's protocol; RNA concentrations were measured on a NanoDrop ND-1000 spectrophotometer (Thermo Fisher Scientific). The 2200 TapeStation System (Agilent) was applied to validate RNA integrity.

Library preparation. Sequencing libraries from human tissues were prepared as described in Perdikari et al.[36]. Sequencing libraries from mouse tissues were prepared from 10 ng of total RNA (RNA integrity number 7.5–9.4) using the TruSeq Stranded mRNA Library Prep Kit (Illumina). The quality and concentration of next-generation sequencing libraries were verified with the 2200 TapeStation System.

Reverse-transcription qPCR of mouse samples. To synthesize complementary DNA, 500 ng RNA was reverse-transcribed with a High-Capacity cDNA Reverse Transcription Kit (Applied Biosystems) in a total volume of 20 µl. Primers (Supplementary Table 1) were premixed with SYBR Green JumpStart Taq ReadyMix (Sigma-Aldrich); 11-µl aliquots were applied to 96-well Multiplate PCR Plates (Bio-Rad Laboratories). cDNA was diluted 1:10 and 2-µl aliquots were added in triplicates. Thermal cycling conditions were: 2 min at 50 °C; 10 min at 95 °C; and 40 cycles of 15 s at 95 °C and 1 min at 60 °C on a CFX Connect Real-Time System (Bio-Rad Laboratories). The ΔC$_t$ method was used to calculate relative changes in mRNA abundance. The C$_t$ value for transcription initiation factor IIB (TFIIB; *Gtf2b*; *GTF2B*) was subtracted from the C$_t$ value for the target gene to adjust for variations in the efficiency of cDNA synthesis. Thus, the values represent the number of mRNA molecules per *Gtf2b* mRNA molecule (Supplementary Fig. 13).

RNA-Seq. RNA-Seq of human samples was performed as described in Perdikari et al.[36]. The accession number at the European Nucleotide Archive is PRJEB20634.

For the mouse samples, single-read sequencing was performed at the Functional Genomics Center Zurich on an Illumina HiSeq 4000 platform. Reads were quality-trimmed and known Illumina adaptors were removed using Trimmomatic v.0.35 (ref. [65]), with the parameters TruSeq3-SE.fa:2:30:10 LEADING:20 TRAILING:20 SLIDINGWINDOW:4:20 MINLEN:50. Read quality was assessed with FastQC

(http://www.bioinformatics.babraham.ac.uk/projects/fastqc; Babraham Institute). The accession numbers at Array Express are E-MTAB-7561 (iBAT and ingWAT samples from standard and physiologically humanized mice) and E-MTAB-7565 (iBAT and ingWAT samples from cold-acclimated mice).

Processed reads were mapped to the *Mus musculus* GRCm38 and *Homo sapiens* GRCh38 reference genomes (soft-masked primary assemblies), using STAR v.2.5.3a (ref. [66]) with GRCm38.90.chr and GRCh38 GTF annotations from Ensembl (release 90)[67]. BAM files were sorted using SAMtools v.1.6 (ref. [68]) and mapping quality was assessed using QoRTs v.1.1.8 (ref. [69]). Uniquely mapped reads aligning to exons were counted using featureCounts from the Subread package v.1.5.3 (ref. [70]). Subsequent gene expression analyses were performed in R. Orthologous relationships between mouse and human genes were identified using biomaRt v.2.34 (ref. [71]) using the hsapiens_gene_ensembl BioMart database. For the inter-species comparisons, only mouse and human genes with unique orthologues ('one2one') were used (16,771 genes). Therefore, the *P2rx5* and *Cited1* marker genes were not used in the inter-species comparisons.

Counts per million (cpm) were calculated with EdgeR v.3.20 (ref. [72]) using a prior count of 0.25; genes with more than 1 cpm in at least 10 libraries were further considered. Libraries were normalized using the weighted trimmed mean of M-values algorithm, as implemented in EdgeR. The tidyverse v.1.2.1 R packages (https://CRAN.R-project.org/package=tidyverse), Snakemake[73] and Biopython[74] were used for workflow management, data transformations and quality control at multiple steps of the analysis.

Differential gene expression analysis was performed using the DESeq2 algorithm on the RNA-Seq 2G web portal (http://52.90.192.24:3838/rnaseq2g/) on raw read counts. Significantly differentially expressed genes were defined based on adjusted P values < 0.05 and a mean log$_2$ fold change threshold > 1.

Hierarchical cluster analysis was performed on the ClustVis web tool (https://biit.cs.ut.ee/clustvis/) using Euclidean distance and complete linkage based on normalized reads per kilobase million gene expression values.

For the PCA of mouse and human gene expression data, normalized cpm values were used. PCA was performed in MATLAB v.9.4.0.813654 using the pca function. The scores for PC1 and PC2 were plotted. The 67% confidence intervals were presented.

The computational tool PROFAT was used to predict the browning capacity of both human and mouse adipose tissue samples. Data files containing the raw reads count were uploaded.

Venn diagrams were created using Venn Diagram Plotter (https://omics.pnl.gov/software/venn-diagram-plotter; Pacific Northwest National Laboratory).

Immunoblot analysis. The right lobe/pad of the adipose tissues was homogenized in modified radioimmunoprecipitation assay buffer (50 mM Tris HCl, pH 7.4, 1% Triton X-100, 150 mM NaCl, 1 mM EDTA) with freshly added 1 mM Na$_3$VO$_4$, 10 mM NaF and protease inhibitor cocktail (cOmplete Mini; Roche). The homogenates, after freezing (in liquid nitrogen) and defrosting to fully lyse the adipose cells, were centrifuged at 14,000g for 15 min. The top fat layer was discarded and the lysate (infranatant) carefully aspirated using a 1 ml syringe and 27 G needle. The concentration of proteins in the lysate was determined using the Lowry method.

An equal volume of reducing sample buffer (125 mM Tris HCl, pH 6.8, 4% wt/vol SDS, 20% vol/vol glycerol, 100 mM dithiothreitol and 0.1% wt/vol bromophenol blue) was added to each sample. Proteins were separated by SDS-polyacrylamide gel electrophoresis in ordinary 12% polyacrylamide gel (acrylamide/bis-acrylamide, 37.5/1). Proteins were transferred to polyvinylidene difluoride membranes (Bio-Rad Laboratories) in 48 mM Tris HCl, 39 mM glycine, 0.037 wt/vol SDS and 15% vol/vol methanol, using a semi-dry electrophoretic transfer cell (Bio-Rad Trans-Blot SD; Bio-Rad Laboratories) at 1.2 mA cm^{-2} for 90 min. After washing, the membrane was blocked in 5% milk in Tris-buffered Saline-Tween 20 for 1 h at room temperature and probed with the indicated antibodies overnight at 4 °C. The immunoblot was visualized with appropriate horseradish peroxidase-conjugated secondary antibodies and enhanced chemiluminescence (ECL Kit; GE Healthcare Life Sciences) in a charge-coupled device camera (Fujifilm). Full unedited blots are shown in Supplementary Fig. 14. After the results were acquired, membranes were stained with Amido black to check for equal protein loading.

The antibodies used were as follows: UCP1 antibody (rabbit polyclonal, raised against the C-terminal decapeptide; not commercially available) diluted 1:15,000; FABP4 antibody (catalogue no. 3544; Cell Signaling Technology) diluted 1:2,000.

Statistical analysis. Age-matched mice were randomly assigned to treatment groups. Sample sizes were determined on the basis of previous experiments using similar methods. All analysed data were included for statistical analyses. The investigators were not blinded to the treatment groups. Results are reported as the mean ± s.e.m. Two-tailed, unpaired Student's t-tests were used for comparison, as indicated in the figure legends. The statistical differences between iBAT and ingWAT are indicated as *P < 0.05, **P < 0.01 and ***P < 0.001. The statistical differences between humanized and standard conditions are indicated as $^{#}P$ < 0.05, $^{##}P$ < 0.01 and $^{###}P$ < 0.001.

Reporting Summary. Further information on research design is available in the Nature Research Reporting Summary linked to this article.

Data availability

The RNA-Seq data of human samples have been deposited with the European Nucleotide Archive with the accession number PRJEB20634(ref. [36]). The RNA-Seq data of mouse samples have been deposited with Array Express with accession nos. E-MTAB-7561 (iBAT and ingWAT samples from standard and physiologically humanized mice) and E-MTAB-7565 (iBAT and ingWAT samples from cold-acclimated mice).

Code availability

The detailed MATLAB code for the PCA can be obtained upon reasonable request.

References

1. Nedergaard, J., Bengtsson, T. & Cannon, B. Unexpected evidence for active brown adipose tissue in adult humans. *Am. J. Physiol. Endocrinol. Metab.* **293**, E444–E452 (2007).
2. Cypess, A. M. et al. Identification and importance of brown adipose tissue in adult humans. *N. Engl. J. Med* **360**, 1509–1517 (2009).
3. Saito, M. et al. High incidence of metabolically active brown adipose tissue in healthy adult humans: effects of cold exposure and adiposity. *Diabetes* **58**, 1526–1531 (2009).
4. van Marken Lichtenbelt, W. D. et al. Cold-activated brown adipose tissue in healthy men. *N. Engl. J. Med* **360**, 1500–1508 (2009).
5. Virtanen, K. A. et al. Functional brown adipose tissue in healthy adults. *N. Engl. J. Med.* **360**, 1518–1525 (2009).
6. Zingaretti, M. C. et al. The presence of UCP1 demonstrates that metabolically active adipose tissue in the neck of adult humans truly represents brown adipose tissue. *FASEB J.* **23**, 3113–3120 (2009).
7. Saito, M. Brown adipose tissue as a therapeutic target for human obesity. *Obes. Res. Clin. Pract.* **7**, e432–e438 (2013).
8. Harms, M. & Seale, P. Brown and beige fat: development, function and therapeutic potential. *Nat. Med.* **19**, 1252–1263 (2013).
9. Carey, A. L. & Kingwell, B. A. Brown adipose tissue in humans: therapeutic potential to combat obesity. *Pharmacol. Ther.* **140**, 26–33 (2013).
10. Bartelt, A. & Heeren, J. The holy grail of metabolic disease: brown adipose tissue. *Curr. Opin. Lipidol.* **23**, 190–195 (2012).
11. Nedergaard, J. & Cannon, B. The changed metabolic world with human brown adipose tissue: therapeutic visions. *Cell Metab.* **11**, 268–272 (2010).
12. Kokolus, K. M. et al. Baseline tumor growth and immune control in laboratory mice are significantly influenced by subthermoneutral housing temperature. *Proc. Natl Acad. Sci. USA* **110**, 20176–20181 (2013).
13. Tian, X. Y. et al. Thermoneutral housing accelerates metabolic inflammation to potentiate atherosclerosis but not insulin resistance. *Cell Metab.* **23**, 165–178 (2016).
14. Karp, C. L. Unstressing intemperate models: how cold stress undermines mouse modeling. *J. Exp. Med.* **209**, 1069–1074 (2012).
15. Wu, J. et al. Beige adipocytes are a distinct type of thermogenic fat cell in mouse and human. *Cell* **150**, 366–376 (2012).
16. Sharp, L. Z. et al. Human BAT possesses molecular signatures that resemble beige/brite cells. *PLoS One* **7**, e49452 (2012).
17. Jespersen, N. Z. et al. A classical brown adipose tissue mRNA signature partly overlaps with brite in the supraclavicular region of adult humans. *Cell Metab.* **17**, 798–805 (2013).
18. Cypess, A. M. et al. Anatomical localization, gene expression profiling and functional characterization of adult human neck brown fat. *Nat. Med.* **19**, 635–639 (2013).
19. Lidell, M. E. et al. Evidence for two types of brown adipose tissue in humans. *Nat. Med.* **19**, 631–634 (2013).
20. Cannon, B. & Nedergaard, J. Nonshivering thermogenesis and its adequate measurement in metabolic studies. *J. Exp. Biol.* **214**, 242–253 (2011).
21. Fischer, A. W., Cannon, B. & Nedergaard, J. The answer to the question "What is the best housing temperature to translate mouse experiments to humans?" is: thermoneutrality. *Mol. Metab.* **26**, 1–3 (2019).
22. Roh, H. C. et al. Warming induces significant reprogramming of beige, but not brown, adipocyte cellular identity. *Cell Metab.* **27**, 1121–1137.e5 (2018).
23. Hung, C. M. et al. Rictor/mTORC2 loss in the *Myf5* lineage reprograms brown fat metabolism and protects mice against obesity and metabolic disease. *Cell Rep.* **8**, 256–271 (2014).
24. Sanchez-Gurmaches, J., Hung, C. M. & Guertin, D. A. Emerging complexities in adipocyte origins and identity. *Trends Cell Biol.* **26**, 313–326 (2016).
25. Fischer, A. W. et al. UCP1 inhibition in Cidea-overexpressing mice is physiologically counteracted by brown adipose tissue hyperrecruitment. *Am. J. Physiol. Endocrinol. Metab.* **312**, E72–E87 (2017).
26. Guilherme, A. et al. Neuronal modulation of brown adipose activity through perturbation of white adipocyte lipogenesis. *Mol. Metab.* **16**, 116–125 (2018).
27. Abreu-Vieira, G. et al. Cidea improves the metabolic profile through expansion of adipose tissue. *Nat. Commun.* **6**, 7433 (2015).
28. de Jong, J. M., Larsson, O., Cannon, B. & Nedergaard, J. A stringent validation of mouse adipose tissue identity markers. *Am. J. Physiol. Endocrinol. Metab.* **308**, E1085–E1105 (2015).
29. Waldén, T. B., Hansen, I. R., Timmons, J. A., Cannon, B. & Nedergaard, J. Recruited vs. nonrecruited molecular signatures of brown, "brite," and white adipose tissues. *Am. J. Physiol. Endocrinol. Metab.* **302**, E19–E31 (2012).
30. Petrovic, N. et al. Chronic peroxisome proliferator-activated receptor γ (PPARγ) activation of epididymally derived white adipocyte cultures reveals a population of thermogenically competent, UCP1-containing adipocytes molecularly distinct from classic brown adipocytes. *J. Biol. Chem.* **285**, 7153–7164 (2010).
31. Ishibashi, J. & Seale, P. Medicine. Beige can be slimming. *Science* **328**, 1113–1114 (2010).
32. de Jong, J. M. A. et al. The β₃-adrenergic receptor is dispensable for browning of adipose tissues. *Am. J. Physiol. Endocrinol. Metab.* **312**, E508–E518 (2017).
33. Kalinovich, A. V., de Jong, J. M., Cannon, B. & Nedergaard, J. UCP1 in adipose tissues: two steps to full browning. *Biochimie* **134**, 127–137 (2017).
34. Shinoda, K. et al. Genetic and functional characterization of clonally derived adult human brown adipocytes. *Nat. Med.* **21**, 389–394 (2015).
35. Ussar, S. et al. ASC-1, PAT2, and P2RX5 are cell surface markers for white, beige, and brown adipocytes. *Sci. Transl. Med.* **6**, 247ra103 (2014).
36. Perdikari, A. et al. BATLAS: deconvoluting brown adipose tissue. *Cell Rep.* **25**, 784–797.e4 (2018).
37. Lin, S. et al. Comparison of the transcriptional landscapes between human and mouse tissues. *Proc. Natl Acad. Sci. USA* **111**, 17224–17229 (2014).
38. Breschi, A. et al. Gene-specific patterns of expression variation across organs and species. *Genome Biol.* **17**, 151 (2016).
39. Sudmant, P. H., Alexis, M. S. & Burge, C. B. Meta-analysis of RNA-seq expression data across species, tissues and studies. *Genome Biol.* **16**, 287 (2015).
40. Su, A. I. et al. Large-scale analysis of the human and mouse transcriptomes. *Proc. Natl Acad. Sci. USA* **99**, 4465–4470 (2002).
41. Chan, E. T. et al. Conservation of core gene expression in vertebrate tissues. *J. Biol.* **8**, 33 (2009).
42. Jespersen, N. Z. et al. Heterogeneity in the perirenal region of humans suggests presence of dormant brown adipose tissue that contains brown fat precursor cells. *Mol. Metab.* **24**, 30–43 (2019).
43. Shabalina, I. G. et al. UCP1 in brite/beige adipose tissue mitochondria is functionally thermogenic. *Cell Rep.* **5**, 1196–1203 (2013).
44. Cheng, Y. et al. Prediction of adipose browning capacity by systematic integration of transcriptional profiles. *Cell Rep.* **23**, 3112–3125 (2018).
45. Cannon, B. & Nedergaard, J. Brown adipose tissue: function and physiological significance. *Physiol. Rev.* **84**, 277–359 (2004).
46. Virtue, S. & Vidal-Puig, A. Assessment of brown adipose tissue function. *Front. Physiol.* **4**, 128 (2013).
47. Berry, D. C. et al. Cellular aging contributes to failure of cold-induced beige adipocyte formation in old mice and humans. *Cell Metab.* **25**, 166–181 (2017).
48. Zhang, F. et al. An adipose tissue atlas: an image-guided identification of human-like BAT and beige depots in rodents. *Cell Metab.* **27**, 252–262.e3 (2018).
49. Bonet, M. L., Oliver, P. & Palou, A. Pharmacological and nutritional agents promoting browning of white adipose tissue. *Biochim. Biophys. Acta* **1831**, 969–985 (2013).
50. Wu, J., Cohen, P. & Spiegelman, B. M. Adaptive thermogenesis in adipocytes: is beige the new brown? *Genes Dev.* **27**, 234–250 (2013).
51. Nedergaard, J. & Cannon, B. The browning of white adipose tissue: some burning issues. *Cell Metab.* **20**, 396–407 (2014).
52. Frontini, A. et al. White-to-brown transdifferentiation of omental adipocytes in patients affected by pheochromocytoma. *Biochim. Biophys. Acta* **1831**, 950–959 (2013).
53. van der Lans, A. A. J. J. et al. Cold acclimation recruits human brown fat and increases nonshivering thermogenesis. *J. Clin. Invest.* **123**, 3395–3403 (2013).
54. Yoneshiro, T. et al. Recruited brown adipose tissue as an antiobesity agent in humans. *J. Clin. Invest.* **123**, 3404–3408 (2013).
55. Romu, T. et al. A randomized trial of cold-exposure on energy expenditure and supraclavicular brown adipose tissue volume in humans. *Metabolism* **65**, 926–934 (2016).
56. Puar, T. et al. Genotype-dependent brown adipose tissue activation in patients with pheochromocytoma and paraganglioma. *J. Clin. Endocrinol. Metab.* **101**, 224–232 (2016).
57. Wang, Q. et al. Brown adipose tissue in humans is activated by elevated plasma catecholamines levels and is inversely related to central obesity. *PLoS One* **6**, e21006 (2011).
58. Manieri, M., Murano, I., Fianchini, A., Brunelli, A. & Cinti, S. Morphological and immunohistochemical features of brown adipocytes and preadipocytes in a case of human hibernoma. *Nutr. Metab. Cardiovasc. Dis.* **20**, 567–574 (2010).

59. Gadea, E. et al. Hibernoma: a clinical model for exploring the role of brown adipose tissue in the regulation of body weight? *J. Clin. Endocrinol. Metab.* **99**, 1–6 (2014).

60. Søndergaard, E. et al. Chronic adrenergic stimulation induces brown adipose tissue differentiation in visceral adipose tissue. *Diabet. Med* **32**, e4–e8 (2015).

61. Orava, J. et al. Different metabolic responses of human brown adipose tissue to activation by cold and insulin. *Cell Metab.* **14**, 272–279 (2011).

62. Golozoubova, V. et al. Only UCP1 can mediate adaptive nonshivering thermogenesis in the cold. *FASEB J.* **15**, 2048–2050 (2001).

63. Cinti, S., Zingaretti, M. C., Cancello, R., Ceresi, E. & Ferrara, P. Morphologic techniques for the study of brown adipose tissue and white adipose tissue. *Methods Mol. Biol.* **155**, 21–51 (2001).

64. Petrovic, N., Shabalina, I. G., Timmons, J. A., Cannon, B. & Nedergaard, J. Thermogenically competent nonadrenergic recruitment in brown preadipocytes by a PPARγ agonist. *Am. J. Physiol. Endocrinol. Metab.* **295**, E287–E296 (2008).

65. Bolger, A. M., Lohse, M. & Usadel, B. Trimmomatic: a flexible trimmer for Illumina sequence data. *Bioinformatics* **30**, 2114–2120 (2014).

66. Dobin, A. et al. STAR: ultrafast universal RNA-seq aligner. *Bioinformatics* **29**, 15–21 (2013).

67. Zerbino, D. R. et al. Ensembl 2018. *Nucleic Acids Res.* **46**, D754–D761 (2018).

68. Li, H. et al. The sequence alignment/map format and SAMtools. *Bioinformatics* **25**, 2078–2079 (2009).

69. Hartley, S. W. & Mullikin, J. C. QoRTs: a comprehensive toolset for quality control and data processing of RNA-Seq experiments. *BMC Bioinformatics* **16**, 224 (2015).

70. Liao, Y., Smyth, G. K. & Shi, W. featureCounts: an efficient general purpose program for assigning sequence reads to genomic features. *Bioinformatics* **30**, 923–930 (2014).

71. Durinck, S., Spellman, P. T., Birney, E. & Huber, W. Mapping identifiers for the integration of genomic datasets with the R/Bioconductor package biomaRt. *Nat. Protoc.* **4**, 1184–1191 (2009).

72. Robinson, M. D., McCarthy, D. J. & Smyth, G. K. edgeR: a Bioconductor package for differential expression analysis of digital gene expression data. *Bioinformatics* **26**, 139–140 (2010).

73. Köster, J. & Rahmann, S. Snakemake—a scalable bioinformatics workflow engine. *Bioinformatics* **28**, 2520–2522 (2012).

74. Cock, P. J. et al. Biopython: freely available Python tools for computational molecular biology and bioinformatics. *Bioinformatics* **25**, 1422–1423 (2009).

Author contributions

J.J., J.N., C.W. and N.P. designed the research. J.J., W.S., A.Frontini, A.W.F. and N.P. performed the experiments. J.J., W.S., N.D.P., M.B., K.P., A.Feizi, M.H.B. and N.P. performed the bioinformatics analyses. A.Frontini, T.N., P.N., S.C., K.V., N.Z.J., S.N., C.S. and C.W. provided essential materials and made comments on the manuscript. J.J., B.C., J.N. and N.P. wrote the manuscript. N.P. supervised the research.

Competing interests

The authors declare no competing interests.

Additional information

Supplementary information is available for this paper at https://doi.org/10.1038/s42255-019-0101-4.

Reprints and permissions information is available at www.nature.com/reprints.

Correspondence and requests for materials should be addressed to N.P.

Peer review information: Primary Handling Editor: Elena Bellafante.

Publisher's note: Springer Nature remains neutral with regard to jurisdictional claims in published maps and institutional affiliations.

nature research

Corresponding author(s):	Natasa Petrovic
Last updated by author(s):	Jan 17, 2019

Reporting Summary

Nature Research wishes to improve the reproducibility of the work that we publish. This form provides structure for consistency and transparency in reporting. For further information on Nature Research policies, see Authors & Referees and the Editorial Policy Checklist.

Statistics

For all statistical analyses, confirm that the following items are present in the figure legend, table legend, main text, or Methods section.

n/a	Confirmed	
☐	☒	The exact sample size (*n*) for each experimental group/condition, given as a discrete number and unit of measurement
☐	☒	A statement on whether measurements were taken from distinct samples or whether the same sample was measured repeatedly
☐	☒	The statistical test(s) used AND whether they are one- or two-sided *Only common tests should be described solely by name; describe more complex techniques in the Methods section.*
☒	☐	A description of all covariates tested
☒	☐	A description of any assumptions or corrections, such as tests of normality and adjustment for multiple comparisons
☐	☒	A full description of the statistical parameters including central tendency (e.g. means) or other basic estimates (e.g. regression coefficient) AND variation (e.g. standard deviation) or associated estimates of uncertainty (e.g. confidence intervals)
☒	☐	For null hypothesis testing, the test statistic (e.g. *F*, *t*, *r*) with confidence intervals, effect sizes, degrees of freedom and *P* value noted *Give P values as exact values whenever suitable.*
☒	☐	For Bayesian analysis, information on the choice of priors and Markov chain Monte Carlo settings
☒	☐	For hierarchical and complex designs, identification of the appropriate level for tests and full reporting of outcomes
☒	☐	Estimates of effect sizes (e.g. Cohen's *d*, Pearson's *r*), indicating how they were calculated

Our web collection on statistics for biologists contains articles on many of the points above.

Software and code

Policy information about availability of computer code

Data collection	RNA sequencing reads were quality-trimmed and known Illumina adaptors were removed using Trimmomatic 0.35, with the parameters TruSeq3-SE.fa:2:30:10 LEADING:20 TRAILING:20 SLIDINGWINDOW:4:20 MINLEN:50. Read quality was assessed using FastQC (http://www.bioinformatics.babraham.ac.uk/projects/fastqc).
Data analysis	Processed reads were mapped to the Mus musculus GRCm38 and Homo sapiens GRCh38 reference genomes (soft masked primary assemblies), using STAR v2.5.3a with GRCm38.90.chr and GRCh38 GTF annotations from Ensembl. BAM files were sorted using samtools v1.6, and mapping quality was assessed using QoRTs. Uniquely mapped reads aligning to exons were counted using featureCounts from the Subread package v1.5.3. Subsequent gene expression analyses were performed in R. Orthologous relationships between mouse and human genes were identified using biomaRt v2.34, using the hsapiens_gene_ensembl BioMart database. For the inter-species comparisons, only mouse and human genes with unique orthologs ('one2one') were used (16771 genes). Counts per million (cpm) were calculated with EdgeR 3.20 using a prior count of 0.25; genes with more than one cpm in at least ten libraries were further considered. Libraries were normalised using the TMM (weighted trimmed mean of M-values) algorithm, as implemented in EdgeR. Tidyverse R packages (https://CRAN.R-project.org/package=tidyverse), Snakemake and Biopython were used for workflow management, data transformations and quality control at multiple steps of the analysis. Differential gene expression analysis was performed using the DESeq2 algorithm on web portal RNA-seq 2G (http://52.90.192.24:3838/rnaseq2g/) on raw reads count. Hierarchical cluster analysis was performed on ClustVis web tool (https://biit.cs.ut.ee/clustvis/) using Euclidean distance and complete linkage based on normalized rpkm gene expression values. For principal component analysis (PCA) of mouse and human gene expression data, normalized cpm values were used. PCA was performed in Matlab (version 9.4.0.813654) using pca function. Scores for component 1 and 2 were plotted. The 67 % confidence intervals were presented.

The computational tool ProFAT (http://profat.genzentrum.lmu.de) was utilized to predict browning capacity of both human and mouse adipose tissue samples.

For manuscripts utilizing custom algorithms or software that are central to the research but not yet described in published literature, software must be made available to editors/reviewers. We strongly encourage code deposition in a community repository (e.g. GitHub). See the Nature Research guidelines for submitting code & software for further information.

Data

Policy information about availability of data

All manuscripts must include a data availability statement. This statement should provide the following information, where applicable:
- Accession codes, unique identifiers, or web links for publicly available datasets
- A list of figures that have associated raw data
- A description of any restrictions on data availability

RNA sequencing data of human samples are deposited at The European Nucleotide Archive with the accession number PRJEB20634. RNA sequencing data of mouse samples are deposited at Array Express with the accession numbers E-MTAB-7561 (IBAT and ingWAT samples from standard and physiologically humanized mice) and E-MTAB-7565 (IBAT and ingWAT samples from cold-acclimated mice).

Field-specific reporting

Please select the one below that is the best fit for your research. If you are not sure, read the appropriate sections before making your selection.

☒ Life sciences ☐ Behavioural & social sciences ☐ Ecological, evolutionary & environmental sciences

For a reference copy of the document with all sections, see nature.com/documents/nr-reporting-summary-flat.pdf

Life sciences study design

All studies must disclose on these points even when the disclosure is negative.

Sample size	Sample sizes were determined on the basis of previous experiments using similar methods.
Data exclusions	All analyzed data were included for statistical analyses.
Replication	Experimental findings were verified by biological replicates (the whole experimental setup (treatment of mice) was repeated and some parameters examined) and by technical replicates (e.g. repeated cDNA synthesis, triplicate measurements of the same sample in qPCR analysis, several gel runs for the same samples in Western blot analysis).
Randomization	Mice from the same litters were put into different groups. The samples from different groups were analyzed in parallel but were run randomly on the gels or qPCR reaction plates.
Blinding	The investigators were not blinded to the mice as they themselves were treating and sacrificing the mice. However, the investigators tended to analyze the samples blindly.

Reporting for specific materials, systems and methods

We require information from authors about some types of materials, experimental systems and methods used in many studies. Here, indicate whether each material, system or method listed is relevant to your study. If you are not sure if a list item applies to your research, read the appropriate section before selecting a response.

Materials & experimental systems

n/a	Involved in the study
☐	☒ Antibodies
☒	☐ Eukaryotic cell lines
☒	☐ Palaeontology
☐	☒ Animals and other organisms
☐	☒ Human research participants
☒	☐ Clinical data

Methods

n/a	Involved in the study
☒	☐ ChIP-seq
☒	☐ Flow cytometry
☒	☐ MRI-based neuroimaging

Antibodies

Antibodies used	Anti-UCP1 antibody, rabbit, polyclonal, raised against C-terminal decapeptide. Anti-FABP4, rabbit monoclonal, clone D25B3, Cell Signaling, Cat No. #3544; Anti-Perilipin-1 antibody, goat, polyclonal, Abcam, Cat No. ab61682.

| Validation | Anti-UCP1 antibody specificity was validated by using the lysates of brown fat from UCP1-knockout mice. Anti-FABP4 antibody and anti-perilipin antibody were validated by the companies. |

Animals and other organisms

Policy information about studies involving animals; ARRIVE guidelines recommended for reporting animal research

Laboratory animals	C57Bl/6 male mice were used. The age of mice varied in different experiments. When sacrificed, "standard" mice were 8 weeks old, cold acclimated mice were approximately 15 weeks old while humanized mice were at least 9 months old.
Wild animals	n/a
Field-collected samples	n/a
Ethics oversight	All experiments were approved by the Animal Ethics Committee of the North Stockholm region.

Note that full information on the approval of the study protocol must also be provided in the manuscript.

Human research participants

Policy information about studies involving human research participants

Population characteristics	Supraclavicular fat for morphological examination was collected during cadaveric examination. The subject was a male, 21 years old (healthy) and with a BMI of 22. Human BAT and WAT biopsies for RNA sequencing analysis were obtained from the supraclavicular region of healthy subjects.
Recruitment	All subjects were healthy volunteers.
Ethics oversight	The study protocol was approved by the Ethics Committee of the Hospital District of Southwest Finland and conducted according to the principals of the Declaration of Helsinki.

Note that full information on the approval of the study protocol must also be provided in the manuscript.